

4.2 Global ocean wave hindcast

4.2.1 Outline of the hindcast

Table 4.3 shows the outline of the global ocean wave hindcast for 10 years from 1980 to 1989. The area of calculation is the whole globe except for high latitudes above 70 degrees, and the grid size is 2.5 degrees in both latitude and longitude (Figure 4.7). The timestep interval $\Delta t = 30$ minutes is chosen so as to satisfy the stability condition of the finite difference scheme. For the longest period $T = 28.6$ seconds of the spectral components of the JWA3G model, $\mu \equiv C_g/R \cdot \Delta t/\Delta x \approx 0.14$ means that the scheme will be stable.

The calculation is carried out for a month, and the two-dimensional wave spectra at all grid points on the last day are adopted as the initial conditions for the calculation of the next month. With respect to the initial condition at January 1980, the JONSWAP spectrum is temporarily adopted, and the wave field for January 1980 is re-calculated using the averaged two-dimensional wave spectra for the last day in December.

The analyzed surface wind field from ECMWF is applied to the hindcast. The wind data have a grid size of 2.5 degrees intervals and the data are available every 12 hours (00Z, 12Z). For the period of 1980-1984, sea surface wind is estimated from the 1000 hPa wind as shown in the next section. After 1985, the analyzed sea surface wind at 10 m height is used directly. The wind input data for the wave model are the linearly interpolated data of ECMWF winds every 12 hours. The sea surface wind at 10 m height u_{10} is converted into the friction velocity u_* by using the equations (3.10)-(3.11) (Wu, 1980).

The monthly mean distribution of sea ice is introduced. If an area previously covered with sea ice becomes open sea, the JONSWAP spectrum is adopted as the initial spectrum in that area. If an area of open sea becomes covered with sea ice, the initial spectrum in the area is set to zero in the same way as the land area.

The wave parameters (wave height, momentum period, peak period and dominant wave direction), which were defined in section 3.6, are calculated from the two-dimensional wave spectra every 6 hours.

4.2.2 Conversion from 1000 hPa wind to sea surface wind

The conversion method from 1000 hPa wind to sea surface wind at 10 m height, which is applied to the wind data before 1985, is described in this section.

It is well-known that the profile of mean wind speed in the surface layer is nearly logarithmic with height under neutral conditions in the surface layer. The logarithmic profile is a function of surface roughness and friction velocity, so the sea surface wind is not able to be estimated directly from the data elements at 1000 hPa. However, the logarithmic law shows the increasing of wind speed at high altitude. Relations between the sea surface wind from NOAA buoys in the north Pacific Ocean and the height of the 1000 hPa isobaric surface are shown in Figures 4.8 and 4.9.

The relation between the wind-direction difference and the height of the 1000 hPa surface comes from the Ekman layer effect, namely, that the wind direction at 1000 hPa rotates clockwise when the height of 1000 hPa is greater than zero. Since the Ekman layer effect depends on the depth of the layer and on the Coriolis parameter, the relation using the NOAA buoy data in the north Pacific Ocean can not be applied to the whole globe. Therefore no conversion of the wind direction from 1000 hPa to sea surface is applied.

It can be considered that the relation between the wind-speed difference and the height of 1000 hPa does not vary with location, except for the stability. The relation is obtained by means of the method of least squares as

$$\frac{U_{1000}}{U_{sf}} = \begin{cases} 0.45 \times (Z_{1000} - 10) / 1000 + 1.09 & (Z_{1000} \geq 10), \\ 1.09 & (Z_{1000} < 10), \end{cases} \quad (4.1)$$

where U_{1000} is the wind speed at 1000 hPa, U_{sf} the wind speed at the sea surface and Z_{1000} is the height of the 1000 hPa isobaric surface in meters. Equation (4.1) is indicated by a broken line in Figure 4.8.

The conversion method is verified by the 1000 hPa wind U_{1000} and sea surface wind U_{sf} from ECMWF. The results are shown in Figures 4.10, 4.11 and 4.12. Figure 4.10 shows the relation between U_{1000} and U_{sf} . It is clear that U_{1000} is greater than U_{sf} . Figure 4.11 shows the relation between U_{sf} and the guessed wind speed U_{guess} from equation (4.1). The converted wind speed agrees well with the sea surface wind speed.

Table 4.3 Outline of global ocean wave hindcast.

Period of calculation	January 1980 - December 1989
Area of calculation	Whole globe exclusive of high latitudes above 70 degrees
Grid interval	2.5 degrees in both latitude and longitude
Time step interval	$\Delta t = 30 \text{ min}$
Initial condition	Wave spectra from the last day of the previous month are set as the initial wave spectra except for January 1980. In January 1980, averaged wave spectra from the last day in December 1980-1989 is adopted.
Wind input data	Objective analysis data by ECMWF Before 1985, surface wind is estimated from 1000hPa wind. After 1985, analyzed surface wind at 10m height is used.
Distribution of sea ice	Monthly mean distribution of sea ice obtained from the published data of Japan Meteorological Agency
Output data of wave model	Wave parameters at all grid points every 6 hours. (Significant wave height, peak and momentum period, dominant wave direction and wave height, period and direction of swell and wind wave components, and also wave height and period of each 12 directions) Wave spectrum at buoy points every 12 hours.

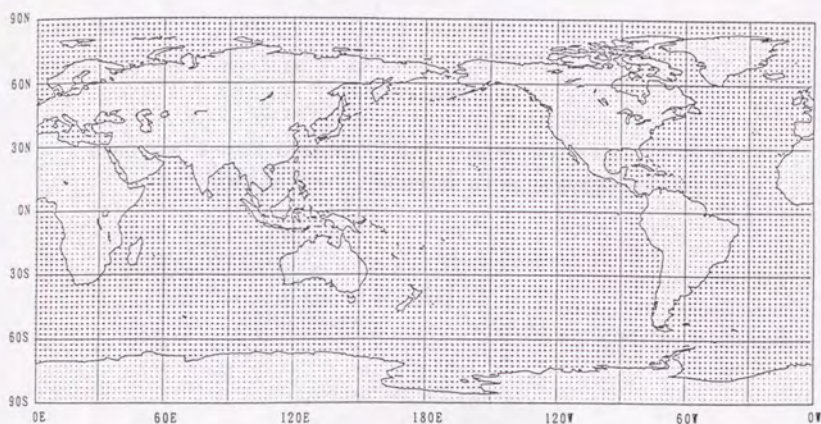


Figure 4.7 Land and sea distribution for calculating the global ocean wave field. Grid size is 2.5 degrees in both latitude and longitude.

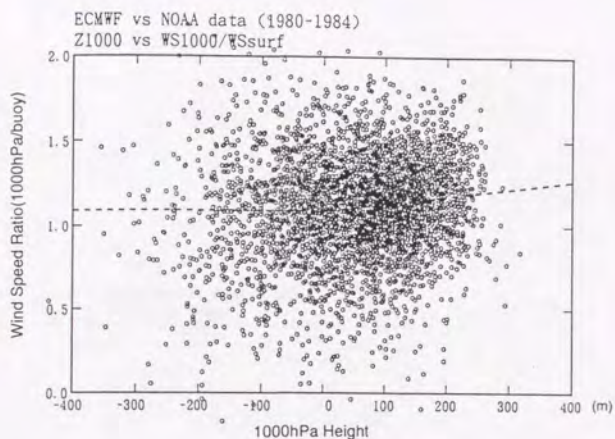


Figure 4.8 Relation between 1000hPa height and ratio of wind speed (1000hPa / buoy). Dashed line shows the equation (4.1).

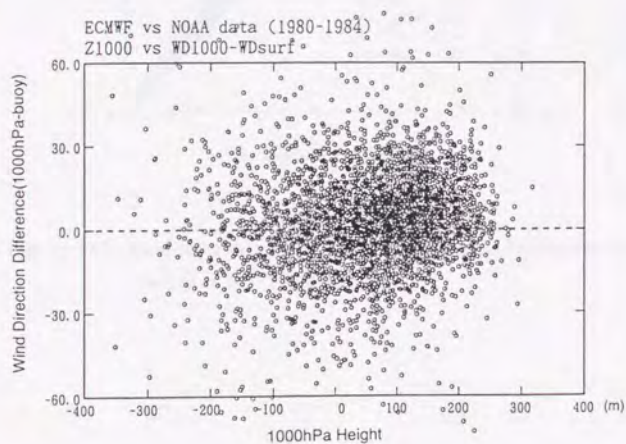


Figure 4.9 Relation between 1000hPa height and difference of wind direction (1000hPa - buoy). Dashed line shows the difference is zero.

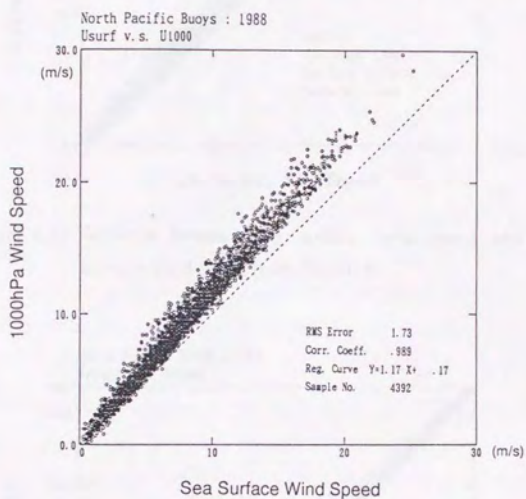


Figure 4.10 Relation between sea surface wind speed and 1000hPa wind speed in ECMWF analysis data.

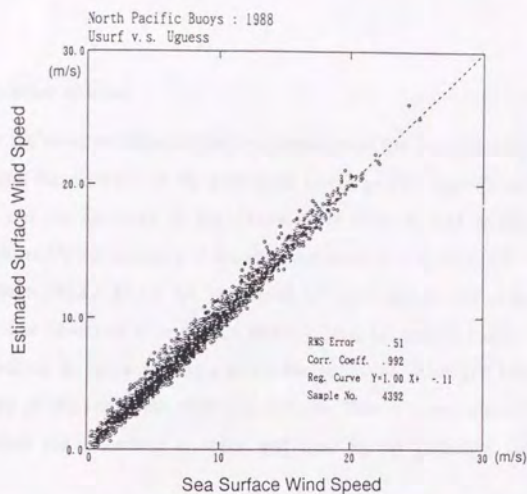


Figure 4.11 Relation between sea surface wind speed and estimated surface wind speed from 1000hPa.

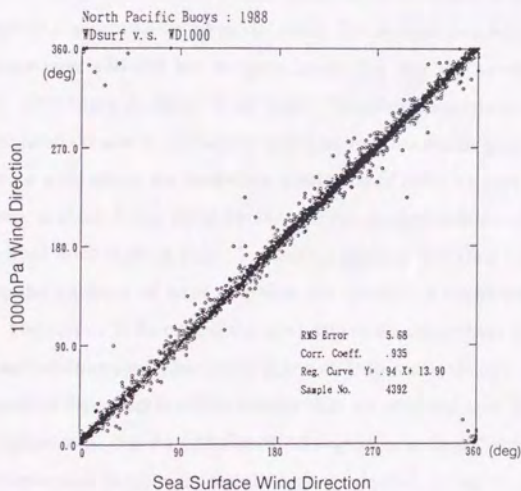


Figure 4.12 Relation between wind direction at sea surface and 1000hPa.

4.3 Verification of wind

Since the wave model calculates the evolution of the wave field by using wind as a forcing term, the accuracy of the calculated waves greatly depends on the accuracy of the wind and the accuracy of the waves never exceeds that of the wind. So it is necessary to verify the accuracy of the analyzed wind data by ECMWF. It must be noted that data from NOAA buoys has been used as input data for the objective analysis of ECMWF. The observed data do not directly become analyzed data themselves, but averaged values in space and time using the predicted value just before the analysis becomes the product from the objective analysis. Thus it is important to verify how the observed data are smoothed in space and time by the objective analysis model of ECMWF.

Figures 4.13, 4.14 and 4.15 show the comparison of the wind data from 1980 to 1989 adopted in JWA3G with the observed wind data from NOAA buoys in the north Pacific Ocean and the north Atlantic Ocean and JMA buoys. The buoy-observed wind speed is converted to the equivalent wind speed at 10 m height. Wind data averaged over 6 hours are compared with the model result. The average over 6 hours corresponds to the average over 180-240 km in space, supposing that the moving speed of the atmospheric disturbance is about 30-40 km/h. Therefore comparison of the averaged data with the model results at 2.5 degrees intervals becomes meaningful. In regard to the accuracy of the wind speed, the correlation coefficient of NOAA buoys is about 0.8 and the RMS error is about 2 m/s, while for JMA buoys, the correlation coefficient is about 0.7 and the RMS error is about 3 m/s. There is no apparent bias error in the wind speed. In regard to the accuracy of wind direction, the correlation coefficients of all buoys exceed 0.9. Therefore it is found that the wind data of the model have slight differences from the observed buoy data. The comparison with JMA buoys (Figure 4.15) shows that the wind speed of the model is a little smaller than the observed one. The cause of that can be considered to be that the grid size of 2.5 degrees is so large for expressing small-scale phenomena such as typhoons that the high wind speed caused by a typhoon is not expressed well.

Tables 4.4 and 4.5 show the year-by-year comparison between model results and buoy data. The accuracy of wind in the model becomes higher with the years, especially

in the latest year 1989, the RMS error of wind speed becomes under 2 m/s. The reason for improvement of the accuracy comes from the improvement of the objective analysis model in ECMWF. The effect of conversion from 1000 hPa wind to surface wind is small, because there has been no particular change in the accuracy of wind since 1985. So it is found that the estimated surface wind data have enough accuracy to calculate the ocean wave field. But it must be noted that the accuracy of the wind changes year by year, so that the accuracy of calculated wave fields using these wind data also changes year by year. On this point, a re-analysis project in ECMWF has already started, by which atmospheric data are being re-analyzed applying the latest objective analysis model for the period 1979-1993 with a resolution of 1 degree in latitude and longitude (Gibson *et al.*, 1994). Once the project is finished, uniformly accurate surface wind data will be available for the calculation of wave fields.

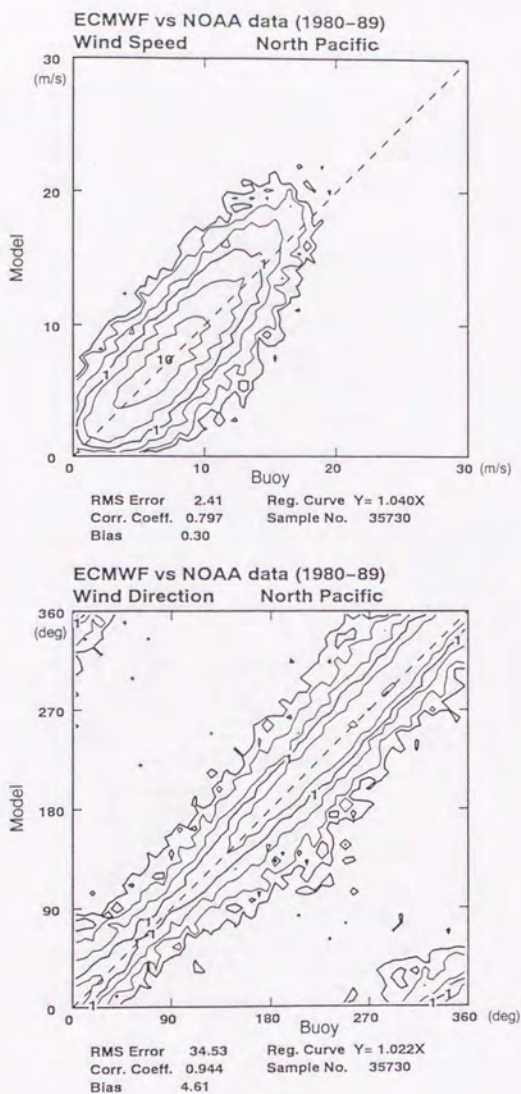


Figure 4.13 Comparison of wind speed of the model with that of the buoy (upper), and comparison of wind direction (lower) at north Pacific Ocean buoys.

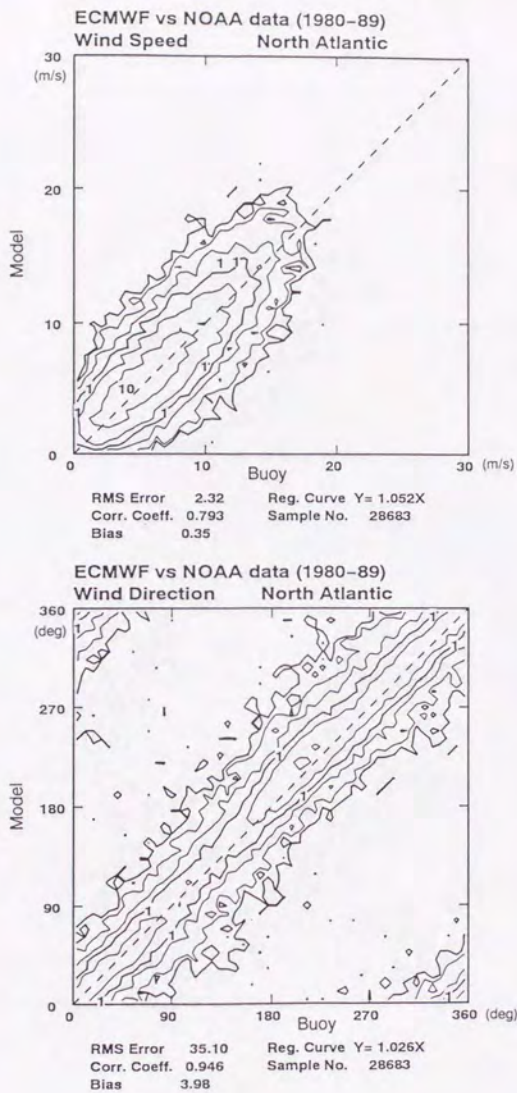


Figure 4.14 Same as Figure 4.13, but for the comparison at north Atlantic Ocean buoys.

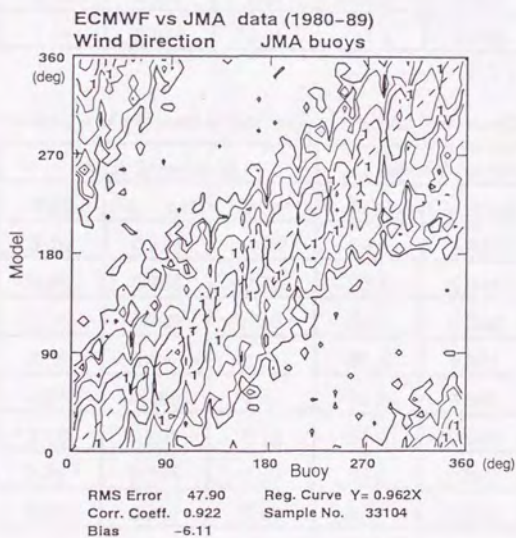
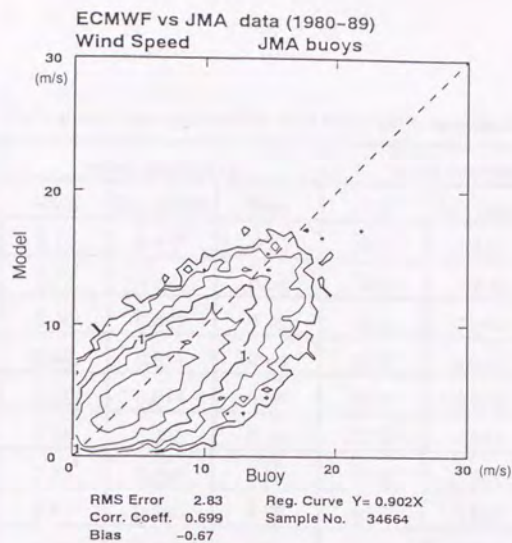


Figure 4.15 Same as Figure 4.13, but for the comparison at JMA buoys.

Table 4.4 Verification of estimated surface wind with NOAA buoy data(North Pacific).

Variable	Wind Speed(m/s)			Wind Direction(deg)		
	RMS	Cor. Coeff.	Bias	RMS	Cor. Coeff.	Bias
1980	3.12	0.675	-0.63	38.9	0.933	7.0
1981	2.77	0.722	0.56	38.6	0.928	5.0
1982	2.40	0.821	0.45	33.5	0.953	6.2
1983	2.42	0.811	0.40	33.8	0.944	4.1
1984	2.39	0.814	0.56	36.6	0.935	8.2
1985	2.25	0.805	0.16	32.6	0.951	1.2
1986	2.35	0.796	0.53	34.6	0.947	6.2
1987	2.11	0.840	0.39	32.9	0.950	4.7
1988	2.19	0.837	0.30	31.5	0.942	1.7
1989	1.84	0.844	0.19	31.1	0.956	1.4

Table 4.5 Verification of estimated surface wind with NOAA buoy data(North Atlantic).

Variable	Wind Speed(m/s)			Wind Direction(deg)		
	RMS	Cor. Coeff.	Bias	RMS	Cor. Coeff.	Bias
1980	3.10	0.756	-1.42	39.6	0.934	8.8
1981	2.76	0.765	0.70	35.9	0.944	1.4
1982	2.38	0.799	0.56	35.3	0.948	6.9
1983	2.38	0.812	0.71	35.5	0.944	3.2
1984	2.26	0.795	0.42	33.9	0.949	4.9
1985	2.16	0.794	0.10	33.1	0.946	3.2
1986	2.25	0.786	0.56	39.2	0.940	1.2
1987	2.01	0.844	0.43	32.6	0.958	2.8
1988	2.01	0.822	0.34	32.4	0.953	4.8
1989	1.98	0.846	0.21	34.0	0.946	3.7

4.4 Case studies of north Pacific Ocean storms

In preparation for an extensive hindcast study of the global ocean wave field over 10 years, two case studies of north Pacific Ocean storms are discussed in this section. The following two cases are studied.

Case 1: The case for the period of 1988 1/12 ~ 1/13

Case 2: The case for the period of 1988 4/15 ~ 4/16

Case 1 is an example in which the evolution of the wave field at buoy 46001 was reproduced well. Case 2 is an example in which a uniquely observed wave with a long wave period of 20 seconds was not calculated by the wave model.

(1) Case 1: The case for the period of 1988 1/12 ~ 1/13

This is a case of the evolution of high waves due to a storm which developed off the Gulf of Alaska. The storm track and the evolution of its central pressure are shown in Figure 4.16. The storm center passes through the vicinity of the west side of buoy 46001 at 12Z on 1/13. The central pressure of the storm reaches 956 hPa at 12Z on 1/12, which corresponds to an intensity comparable with a typhoon. The maximum wind speed becomes about 50 knots (Figure 4.18). Figure 4.17 compares the model results with buoy 46001 data. From the comparison with surface wind, it is found that large-scale phenomena lasting more than a day can be reproduced well by the analyzed wind data from ECMWF. The maximum wind speed at buoy 46001 on 1/12 is about 20 m/s. The wind direction when the maximum wind speed appears is easterly, as the wind direction changes anticlockwise from south due to the passage of the storm on the west side of the buoy. The wave height increases rapidly due to the strong wind and the height reaches about 8 m at 12Z on 1/12.

The wave height calculated by the JWA3G model agrees well with the buoy data. In particular, both the rapid increase of wave height due to a sudden wind increase, and the subsequent decrease in wave height are calculated with high accuracy. The accuracy of wave height in the old first and second generation models were not sufficient, in the case of a rapid increase of the wave height due to a sudden wind increase and the process of decreasing wave height (SWAMP Group, 1985). The reason why the third generation model, represented by JWA3G, has a better accuracy than the old wave

models in case of a sudden increase of the wind is that a highly accurate calculation scheme for the nonlinear energy transfer is implemented in the model. When the wind speed increases suddenly, it can be considered that the increase of wave height comes not only from the energy input by the wind, but also from the nonlinear energy transfer between the existing wave components and the newly-generated wind wave components. Therefore the merit of the third generation wave model shows itself remarkably in this point. The fact that the accuracy of JWA3G in the case of decreasing wave height is better than the old models, indicates that the energy dissipation scheme implemented in the model, in which the experimental $3/2$ power law between wave height and wave period from Toba (1972) is implicitly incorporated, is functioning properly. But the calculated wave period is not so accurate as the wave height, and the phase of changes in the model results lags behind the observation. The wave height parameter is calculated from the 0th moment of the spectrum, while the wave period can be considered to be related to higher-order moments than the 0th moment. So the accuracy of wave period becomes more critical than that of wave height, because the shape of the spectrum is essential.

The distribution of the global wind field, significant wave, wind wave and swell components are shown in Figure 4.18 through Figure 4.21. The mid- and high-latitudes in the north Pacific Ocean form a locality of low pressure and a strong westerly wind blows continuously. The wind-wave component is distributed locally, while the swell component is distributed widely. It can be clearly seen that the swell which is generated by the storm reaches the west coast of United States at 00Z on 1/12 and that there are some swell components propagating far to the southeast beyond the Hawaiian islands across the equator. Just south of the Hawaiian islands, since there always exists a trade wind, wind-wave component with easterly wave direction is remarkable.

The comparison of the calculated wave spectra with observed spectra is shown in Figure 4.22. Although the shape of the spectrum in JWA3G is determined only by the energy balance between source functions, and the prescribed limitation by means of a saturated spectrum is no longer applied, the spectrum of the model agrees well with the observed spectrum and the shape of the equilibrium range is almost proportional to f^{-4} . But some small spectral peaks and a part of the double-peaked spectrum (buoy 46001,

1/12 00Z) in the observed data are not reproduced well.

(2) Case 2: The case for the period of 1988 4/15 ~ 4/16

Case 2 is an example in which a unique long-wave period of more than 20 seconds was observed in several buoys, which can not be reproduced by the model. Earle *et al.* (1984) already reported that this kind of wave with very long wave period was sometimes observed in the area off the Gulf of Alaska and that this wave caused coastal erosion, which is an essential environmental problem.

The storm track and the evolution of its central pressure are shown in Figure 4.23. The storm develops rapidly while moving northeastward at high speed, and turns to the northwest after crossing 50°N. The storm track is nearly the same as in Case 1, but there is a difference that the propagation speed of the storm is high and the development of the storm is rapid. The speed from 4/13 to 4/14 is 60-80 km/h and the central pressure deepens by 32 hPa during the 12 hours from 1/13 12Z to 1/14 00Z. After 1/14, the storm continues to go north while keeping its strength of 960 hPa. Storms which develop rapidly are called "bombs" and are sometimes observed among the storms which pass by the south coast of Japan.

Figure 4.24 compares the model results with buoy 46005 data. No strong wind blows at buoy 46005, since the location of the buoy is far from the storm. However, high wave heights above 5 m are observed from 4/15 to 4/16. The observed peak wave period is more than 20 seconds. These waves are not reproduced well in the model. However, it can be seen in the model results that the area of high swell moves eastward preceding the area of high wind waves (Figures 4.26-4.28), and the swell component reaches the west coast of the United States.

Figure 4.29 shows the comparison of wave spectra in the model with the observed spectra. The observed spectral component with a longer wave period than the calculated one is remarkable at buoys 46004 and 46005. Supposing that the wave is governed by the wind-wave generation mechanism that is typically expressed using Wilson's experimental relations (equations 2.1-2.2), the wave period becomes 20 seconds after a strong wind with a velocity of 40 m/s blows continuously for more than 50 hours over a fetch of 2000 km. If the strong wind blows, the wave height becomes more than 20 m. Earle *et al.* (1984) concluded that the unique phenomenon with very long wave period

was generated due to the effect of moving fetch, in which the apparent fetch length in the forward direction of the storm becomes longer due to the high propagation speed of the storm. If the theory is true, the generated wind wave must increase its wave period gradually and the shape of the spectrum in the equilibrium range must be proportional to f^{-4} . But the observed wave spectrum at buoy 46005 (Figure 4.29) does not have a shape proportional to f^{-4} , so it is possible that the phenomenon occurs due to another mechanism.

Figure 4.30 shows the isochron of the appearance of maximum wave height at each buoy. The difference between the time of appearance of the maximum can be explained well, if a wave packet travels toward the east-northeast direction. The speed of propagation of the wave packet is about 60 km/h based on the isochron intervals. This speed corresponds to the group velocity of deep water waves with a period of about 21 seconds, which is close to the period of the spectral peaks of buoys 46004 and 46005. Therefore it can be considered that the existence of the phenomenon is confirmed. But the generation mechanism is still questionable. According to Figure 4.23, the propagation speed of the storm from 4/13 18Z to 4/14 00Z is about 55 km/h. At that time, the strength of the storm increased rapidly. This propagation speed of the storm almost agrees with that of the wave packet. So it seems probable that the phenomenon with very long wave period is generated by the traveling force due to the sudden change of atmospheric pressure. This kind of problem has been studied since an early date (*e.g.*, Lamb, 1932), but has never been considered as a part of the energy input mechanism in a wave model. If the mechanism is clarified, the dynamic forcing mechanism due to the movement of low pressure areas will have to be incorporated into the energy input mechanism of the wave model.

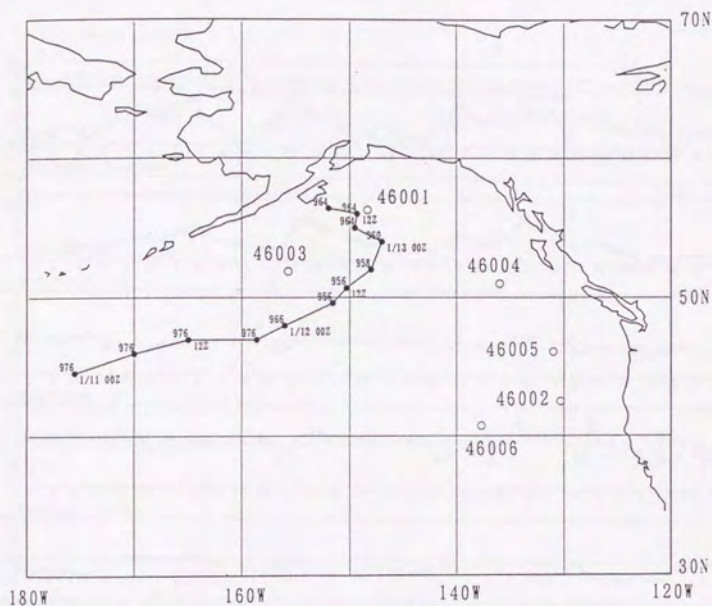


Figure 4.16 Storm track and the central pressure of Case 1 (1988 1/12~13).

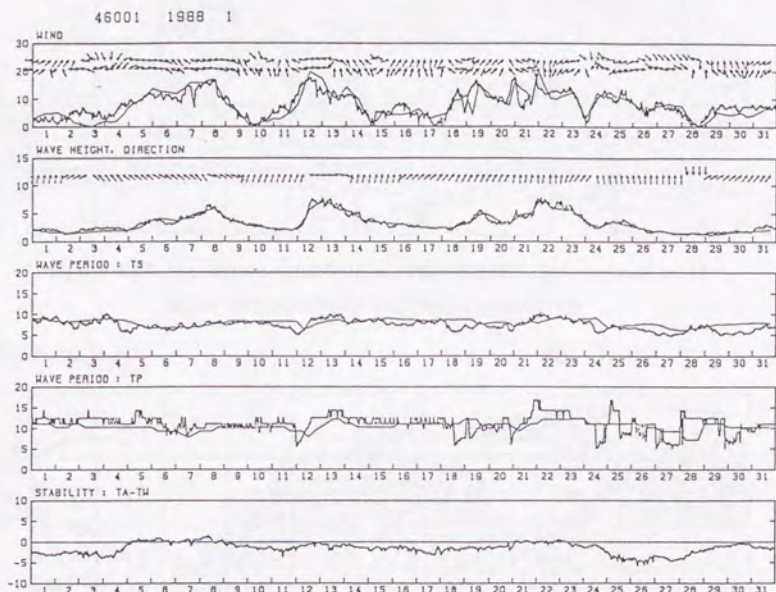


Figure 4.17 Comparison of model results (wind speed and direction, wave height and direction, peak wave period, momentum period and the difference between atmospheric and sea surface temperature) with the observed data at NOAA buoy 46001 in January 1988. The thin lines denote model results and thick lines denote buoy data.

WIND U10

88. 1. 12. 0.

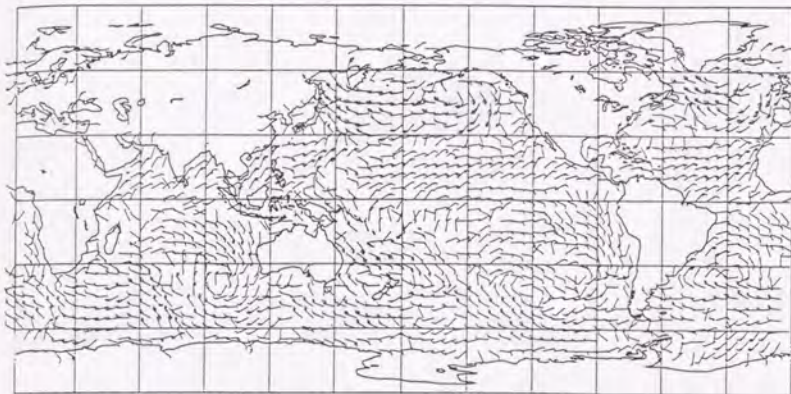


Figure 4.18 Sea surface wind field at 1988 1/12 00Z. Full and half wind barbs correspond to 10 and 5 knots, respectively.

WAVE HEIGHT

88. 1. 12. 0.

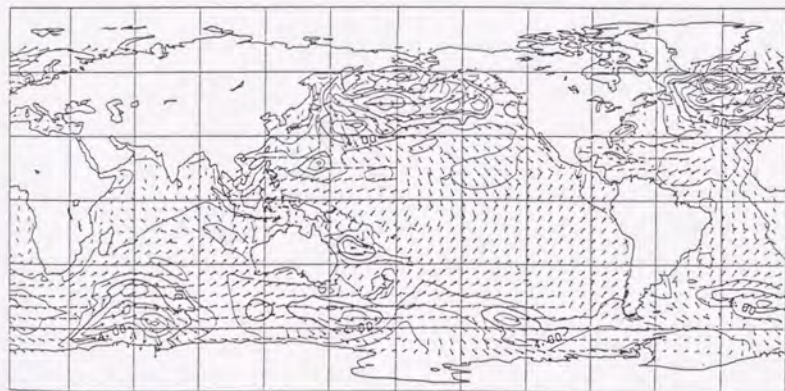


Figure 4.19 Distribution of significant wave height (contour line) and dominant wave direction (arrow) at 1988 1/12 00Z. Contour interval is 1 m.

WIND-WAVE

88. 1. 12. 0.

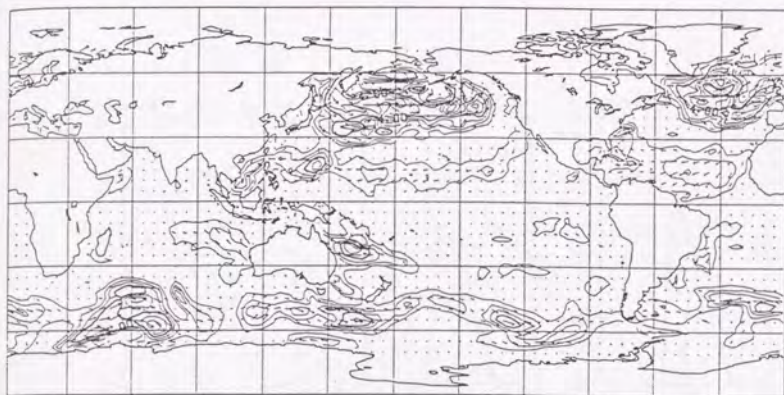


Figure 4.20 Same as Figure 4.19, but for the wind-wave component.

SWELL

88. 1. 12. 0.



Figure 4.21 Same as Figure 4.19, but for the swell component.

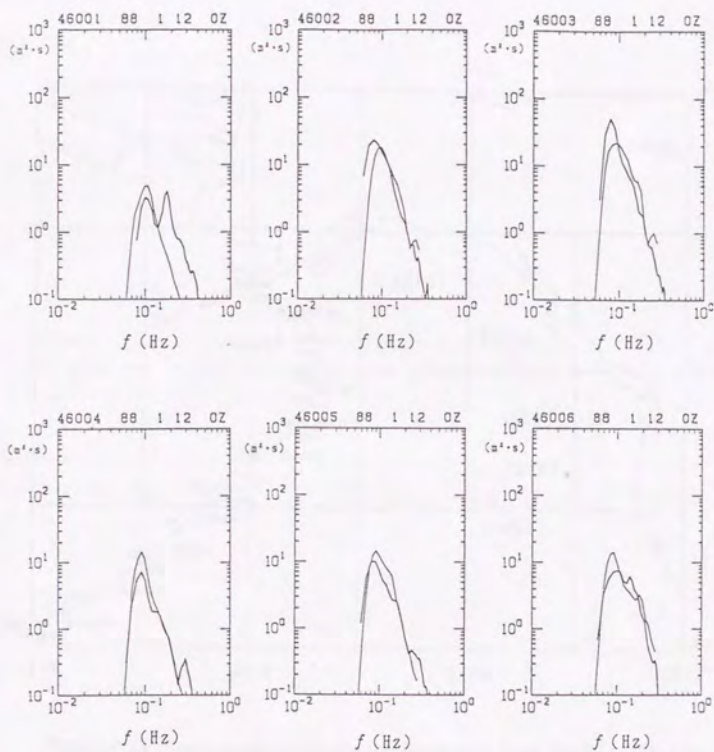


Figure 4.22 Comparison of one-dimensional wave spectra in the model against the observed spectra at 1988 1/12 00Z. Thin lines denote model results and thick lines denote observed data.

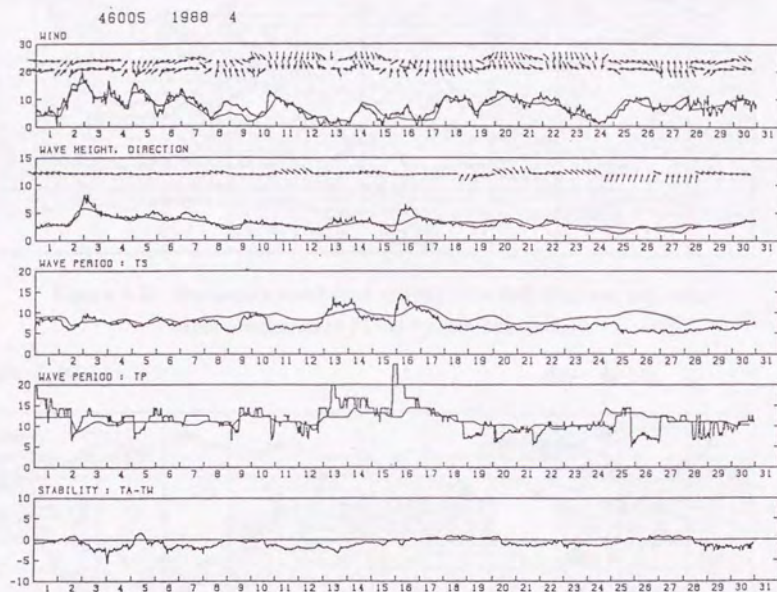


Figure 4.24 Same as Figure 4.17, but for NOAA buoy 46005 in April 1988.

Thin lines denote model results and thick line denote buoy data.

WIND U10

88. 4. 16. 0.

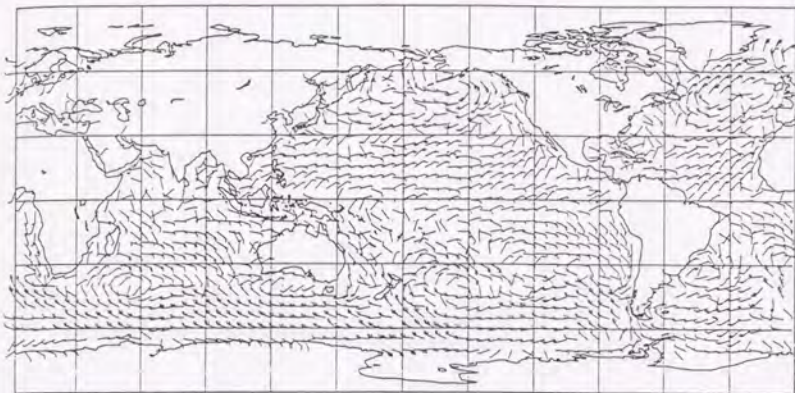


Figure 4.25 Sea surface wind field at 1988 4/16 00Z. Full and half wind barbs correspond to 10 and 5 knots, respectively.

WAVE HEIGHT

88. 4. 16. 0.

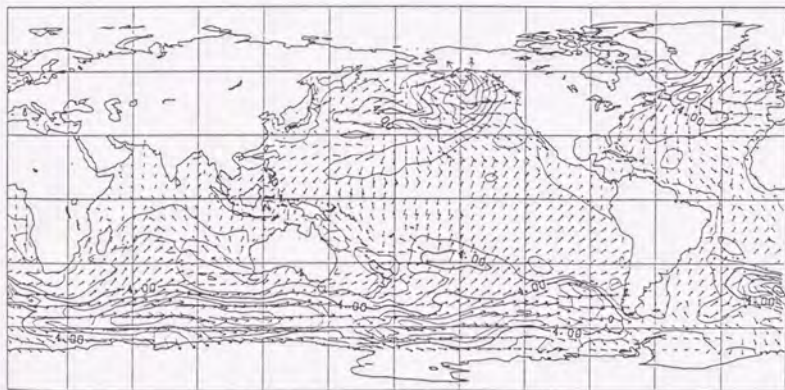


Figure 4.26 Distribution of significant wave height (contour line) and dominant wave direction (arrow) at 1988 4/16 00Z. Contour interval is 1 m.

WIND-WAVE

88. 4. 16. 0.

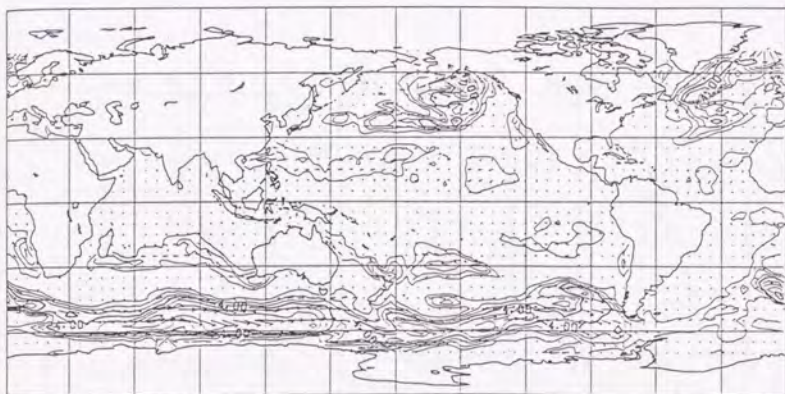


Figure 4.27 Same as Figure 4.26, but for the wind-wave component.

SWELL

88. 4. 16. 0.



Figure 4.28 Same as Figure 4.26, but for the swell component.

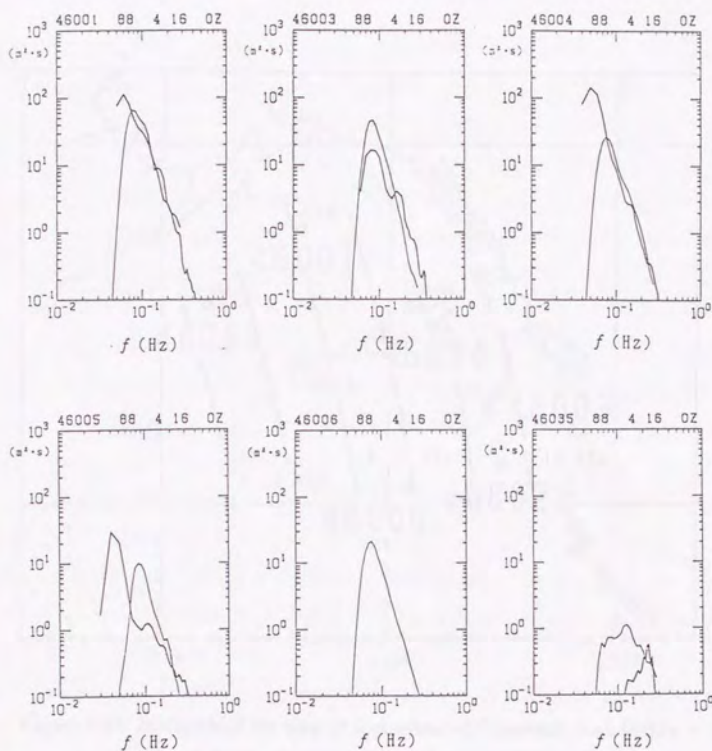


Figure 4.29 Comparison of one-dimensional wave spectra in the model against the observed spectra at 1988 4/16 00Z. Thin lines denote model results and thick lines denote observed data.

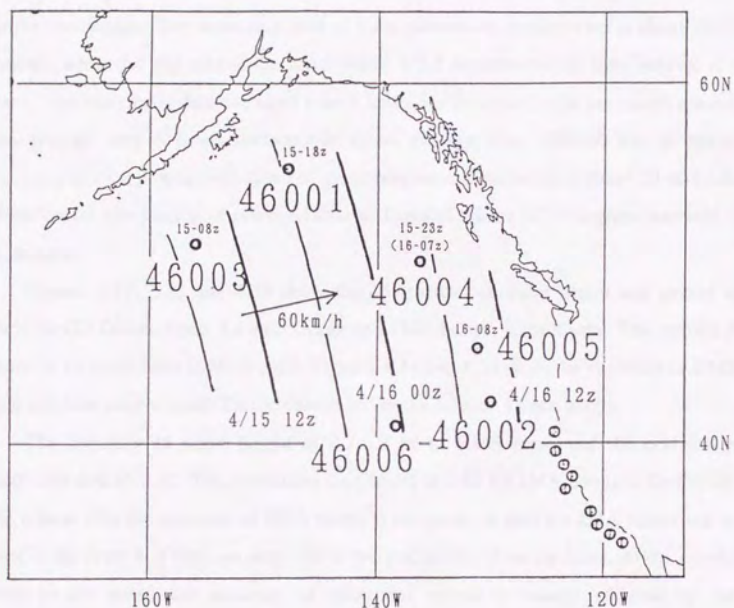


Figure 4.30 Isochrone of the time of appearance of maximum wave height at each buoy. At buoy 46004, the later of two maxima is adopted to draw the isochron. The speed of movement of the isochrone is calculated at about 60 km/h.

4.5 Verification of the hindcast results

4.5.1 Comparison with buoy data

The accuracy of hindcast results for the global ocean wave field is verified by means of comparison with the observed buoy data. NOAA and JMA buoy data are used for the comparison. The measuring time of wave parameters at each buoy is about 10-20 minutes, while the grid size of the wave model is 2.5 degrees and the time interval is 6 hours. Therefore buoy data averaged over 6 hours are compared with the model results. The average over 6 hours corresponds to an average over 180-240 km in space, assuming that the propagation speed of the atmospheric disturbance is about 30-40 km/h. Therefore the comparison of averaged data with model results at 2.5 degrees intervals is meaningful.

Figures 4.31, 4.32 and 4.33 show the comparison of wave height and period at north Pacific Ocean, north Atlantic Ocean and JMA buoys, respectively. The statistical period is 10 years from 1980 to 1989. Figures 4.34 and 4.35 show the variation of RMS error and bias error at north Pacific Ocean and north Atlantic Ocean buoys.

The accuracy of wave height is 0.7-0.9 m in RMS error and the correlation coefficient is 0.65-0.85. The correlation coefficient of 0.65 for JMA buoys is the lowest. The reason why the accuracy at JMA buoys is not good, is that the JMA buoys are so close to the coast that they are only one or two grid points from the coast. At the closest point to the coast, the accuracy of calculated waves is mainly affected by the representation of land-sea distribution. At the north Pacific Ocean buoys, the bias error of wave height is remarkable. The model result is about 50 cm higher than the observed buoy data, while no bias error is found at other buoys. With respect to the wave period, the accuracy is lower than that of wave height at all buoys. The correlation coefficient of wave period is less than 0.5, but this value is a total accuracy of the model. It seems that there are two groups in the comparison of wave period (Figure 4.31). One is the group in which the correlation between model and buoy is good, the other is the group in which the wave period of the model is always longer than in the buoy data. The existence of the longer-period group in the model indicates that the swell component of the model is greater than in the observed buoy data.

The accuracy of wave height varies year by year and becomes higher with the years (Figures 4.34-4.35). The RMS error reduces to about 60 cm in 1989 at both north Pacific and north Atlantic Ocean buoys. However the change of the accuracy at north Pacific Ocean buoys in 1985 is great, while it is small at north Atlantic Ocean buoys. The bias errors before 1985 are about two times as much as those after 1985 at north Pacific Ocean buoys. Two possible explanations for this are suggested. One is that the objective analysis model in ECMWF has been changed year by year, and the other is that the surface wind before 1985 was estimated from 1000 hPa wind. The conversion from 1000 hPa to sea surface was performed as a function of the height of the 1000 hPa level, so that the stability in the atmosphere was not considered. In the stable condition, the effect of vertical diffusion becomes smaller than in the neutral condition, so that the surface wind speed also becomes smaller than that in neutral conditions. While in the unstable condition, the surface wind speed becomes greater than that of neutral conditions due to the effect of active vertical diffusion. However, considering that the change of accuracy is rather greater at north Pacific Ocean buoys than at north Atlantic Ocean buoys, there is a possibility to consider that the analyzed wind field before 1985 has a local difference in its accuracy and wind data in the north Pacific Ocean are less accurate than data in the north Atlantic Ocean.

It is satisfactory to consider that the remarkable bias error at north Pacific Ocean buoys indicates that the energy dissipation of swell components in JWA3G is not enough and the life of swell components from the Antarctic Sea becomes long. The energy dissipation process of JWA3G was determined on the basis of the energy balance between source terms in the equilibrium range of the spectrum. So this energy dissipation scheme was essentially applied only to the equilibrium range, but the scheme was extrapolated to the lower frequency range. Therefore the energy dissipation process in the lower frequency range was not considered enough. From the comparison of wave period, it is found that there is a group in which the period of the model is always longer than in the observed buoy data. The result also shows that the swell component in the model is greater than in the observed data. The insufficient energy dissipation of the swell is a weak point of the JWA3G model at present and it is necessary to improve the model by incorporating some physical process of swell dissipation. Mitsuyasu and

Yoshida (1989) discussed the interaction between swell and wind-wave components on the sea surface where the swell has already existed. They showed that the evolution of wind waves with adverse swell was amplified, while that with favorable swell was suppressed. Phillips and Banner (1974) proposed a mechanism that the evolution of wind waves was suppressed due to the increase of the surface drift near the crests of the swell. If these experimental and theoretical studies are developed, it can be expected that new knowledge about the dissipation of swell will be obtained.

The wave spectrum calculated by the model is compared with the observed spectrum at NOAA buoys in Figures 4.36-4.39. A strong southwest wind with a velocity of about 20 m/s continued to blow from 1/22 to 1/23, which causing wave heights of above 7 m. After 1/24, the wind direction changed to northwest due to the passing of a cold front, so that a wave component in the northwest direction was gradually developed. It is found that the change of the directional spectrum followed well the change of wind direction. A double-peaked spectrum was observed on 1/25, which was also shown by the wave model, but the peak of the wind-wave component is smaller than the observed one. The validity of the separation between swell and wind-wave components is confirmed by Figure 4.39. However the separation is so sensitive to local wind speed that the swell component becomes greater at 1/24 00Z (Figure 4.38) due to the decreasing of wind speed.

The growing spectral peak of wind waves at 1/25 00Z in the model is smaller than in the buoy data, while the peak of swell in the model is a little greater than in the buoy data. The reason is considered as follows. Since analyzed wind data at 12-hour intervals was adopted in the wave model, smaller-scale phenomena than 12 hours, such as a local change of wind, were not able to be expressed by the model. Also the swell dissipation problem in the model caused a difference in the swell component between model results and buoy data. From another viewpoint, if the difference in the swell component is analyzed in detail, it may be that some new knowledge about swell dissipation will be obtained.

4.5.2 Comparison with GEOSAT data

Figures 4.40-4.43 show the comparison of GEOSAT data with model results and buoy data along the orbit path of GEOSAT. As shown in Figure 4.40, it is found that the wave height from the model is always several tens of cm higher than the observed data from GEOSAT in the Pacific Ocean, while the difference between model results and satellite data is very small in the Atlantic Ocean (Figure 4.41), so that the change of wave height in the meridional direction is expressed well by the JWA3G model.

In the case of Figure 4.42, it is found that the sign of the difference between model results and satellite data changes according to the position of the satellite. Not only the bias error in the Pacific Ocean, but also the bias error in the Atlantic Ocean is remarkable. The sign of the bias error in the Atlantic Ocean is opposite to the error in the Pacific Ocean. It is known that there is the Gulf stream in the western boundary of the north Atlantic Ocean and the current speed reaches a maximum of several m/s. As regards the interaction between ocean waves and ocean current, Phillips (1977) showed that the wave action density $F(k)/\omega$, where $F(k)$ is the wave energy and ω is the angular frequency, is conserved along the path of a wave packet traveling with $U + C_g$, where U is the current speed and C_g is the group velocity of the wave component. This mechanism can be considered as a kind of wave refraction, so that the wave energy is changed due to the current speed. If the current speed reduces as a wave packet travels, the wave height becomes higher. Another effect of the interaction between wind and current can be considered. If the wind direction is adverse to the current direction, the wind velocity relative to the sea surface becomes stronger, so that the wave height becomes higher. The wind direction at buoy 41006 in Figure 4.42 is northeast, while the direction of the Gulf stream is southwesterly. In JWA3G, no current effect was considered, so it is possible to consider that the model underestimates the wave height in contrast to the satellite data. However the NOAA buoy observation does not agree with the GEOSAT data, but with model result. So it is difficult to explain the difference between model result and satellite data only by means of the effect of the ocean current.

Figure 4.43 is an example in which typhoon 8713 passed by buoy 21001 of JMA. In this case, a maximum wave height of about 7 m from the model agrees well with that

of the satellite data. Buoy 21001 is located to the east of the center of the typhoon, so the observed wind speed exceeds 30 m/s. Although the 2.5-degree grid size of analyzed wind data by ECMWF is considered to be coarse, a strong typhoon such as this can be resolved well in the ECMWF data.

From the above comparison of model results with GEOSAT data, it is confirmed that although the wave height of the model has a bias error of several tens of cm in the Pacific Ocean, the change of wave height in the meridional direction is expressed well, so that the model has a good accuracy.

Zonal mean wave height against latitude from JWA3G and GEOSAT in 1988 are shown in Figures 4.44 and 4.45. Averaged GEOSAT data on a 2x2-degree grid by Ebuchi *et al.* (1992) are used. The seasonal change of wave height is clearly seen in both figures. In the Antarctic Sea, the wave height reaches about 4 m regardless of the season. In the northern hemisphere, the difference between model results and satellite data is remarkable, and the wave heights from GEOSAT are much smaller than the model results. It is possible that the accuracy of measuring the wave height by the satellite becomes worse when the swell and wind-wave components are overlapping and that the accuracy of the analyzed wind field by ECMWF is not enough. This problem will become clear after further study of the satellite data.

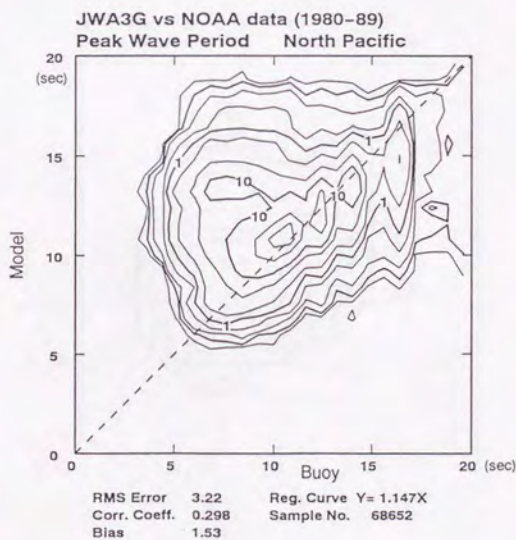
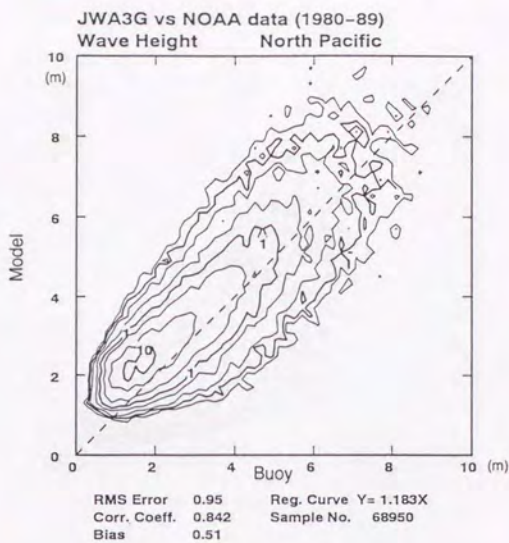


Figure 4.31 Comparison of wave height in the model with that of the buoy (upper), and comparison of wave period (lower) at north Pacific Ocean buoys.

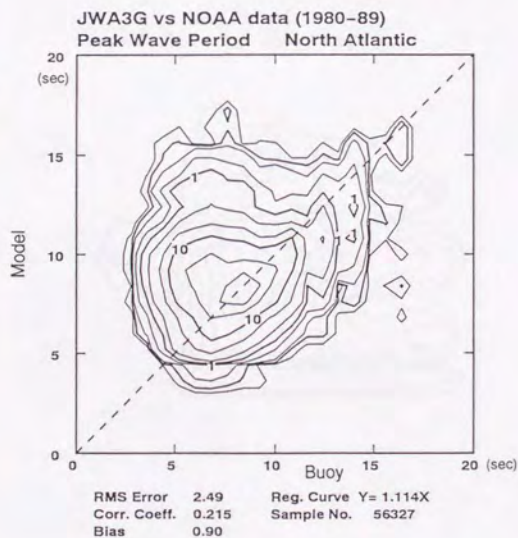
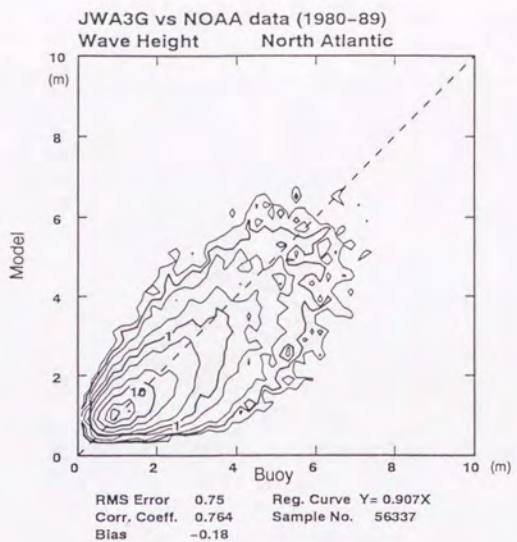


Figure 4.32 Same as Figure 4.31, but for the comparison at north Atlantic Ocean buoys.

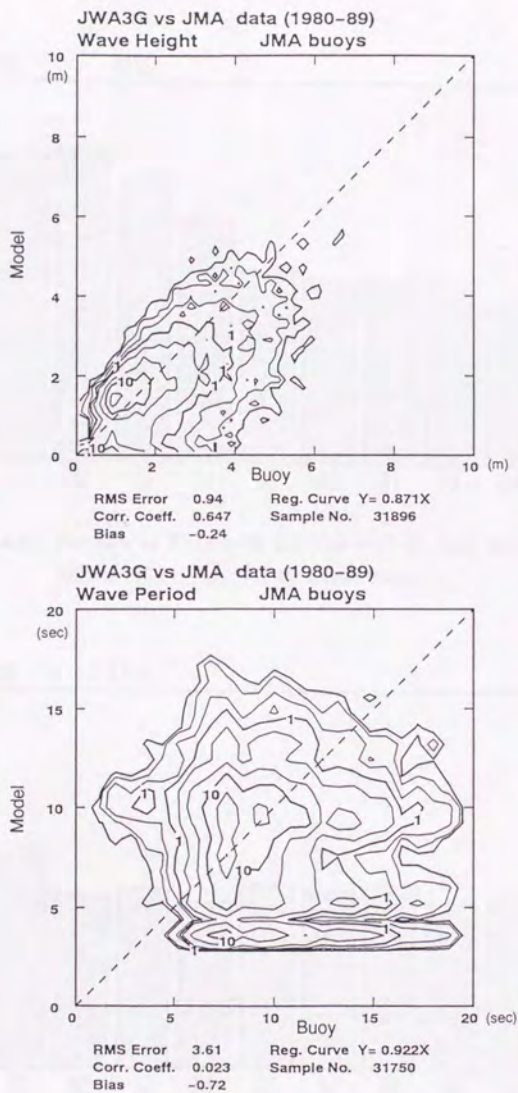


Figure 4.33 Same as Figure 4.31, but for the comparison at JMA buoys.

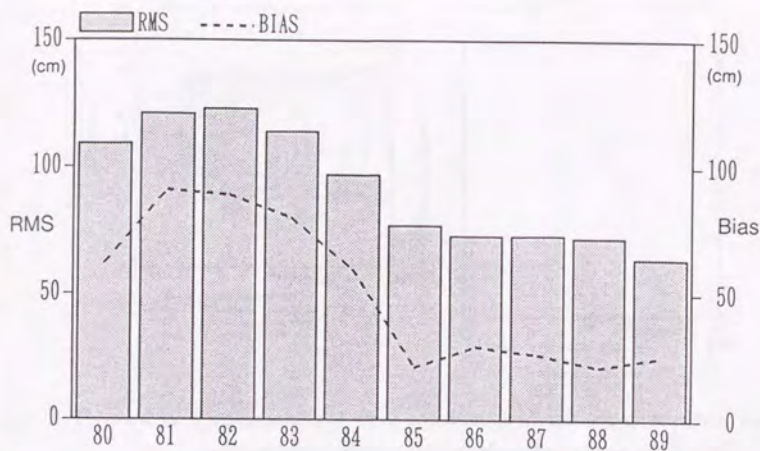


Figure 4.34 Variation of RMS error and bias error of wave height from 1980 to 1989 at north Pacific Ocean buoys.

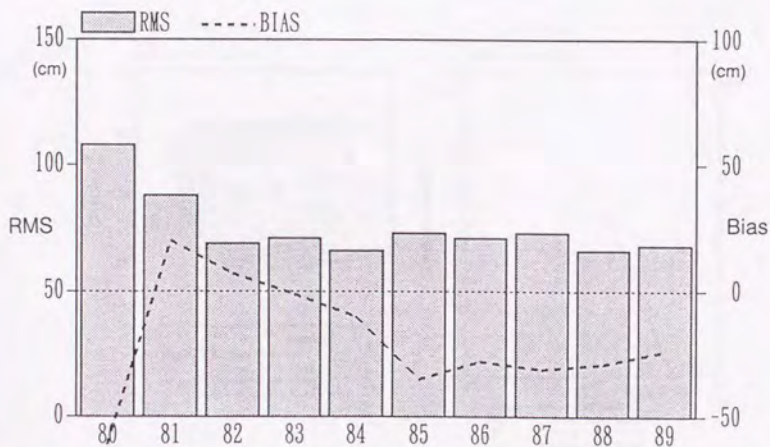


Figure 4.35 Same as Figure 4.34, but for the variation at north Atlantic Ocean buoys.

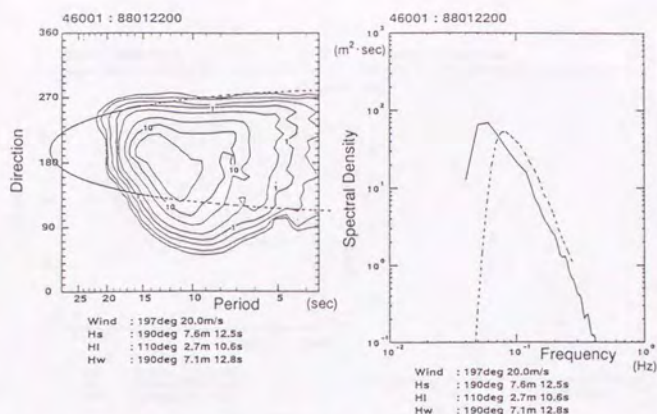


Figure 4.36 Two-dimensional wave spectrum (left) and one-dimensional wave spectrum (right) of the model (dashed line) compared with observed spectrum (solid line) at buoy 46001 at 1988 1/22 00Z, with wave parameters of significant wave (Hs), swell (Hl) and wind wave (Hw). Separation curve between swell and wind-wave components is drawn in the left figure.

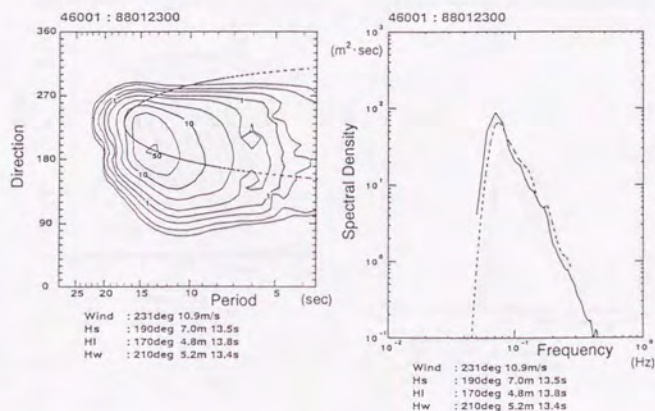


Figure 4.37 Same as Figure 4.36, but for 1988 1/23 00Z.

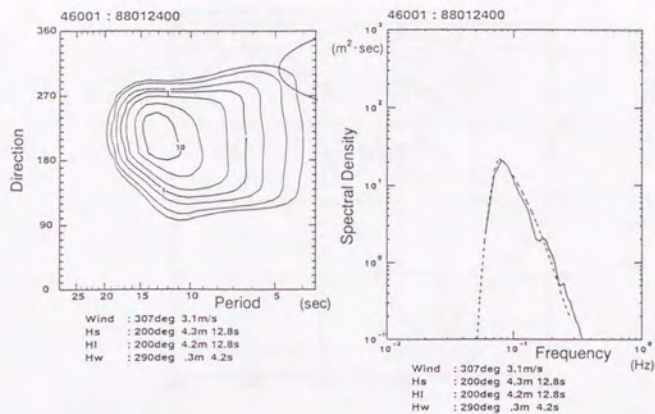


Figure 4.38 Same as Figure 4.36, but for 1988 1/24 00Z.

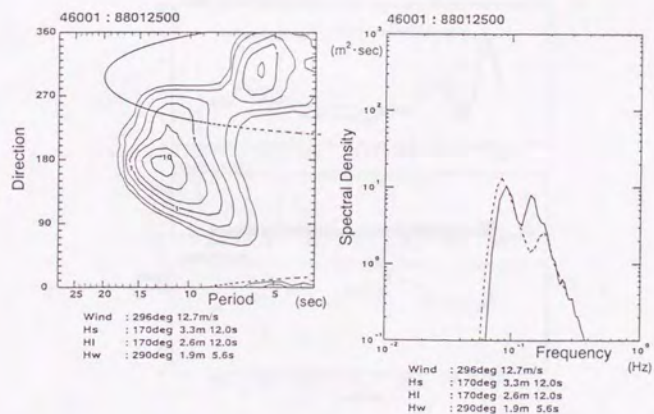


Figure 4.39 Same as Figure 4.36, but for 1988 1/25 00Z.

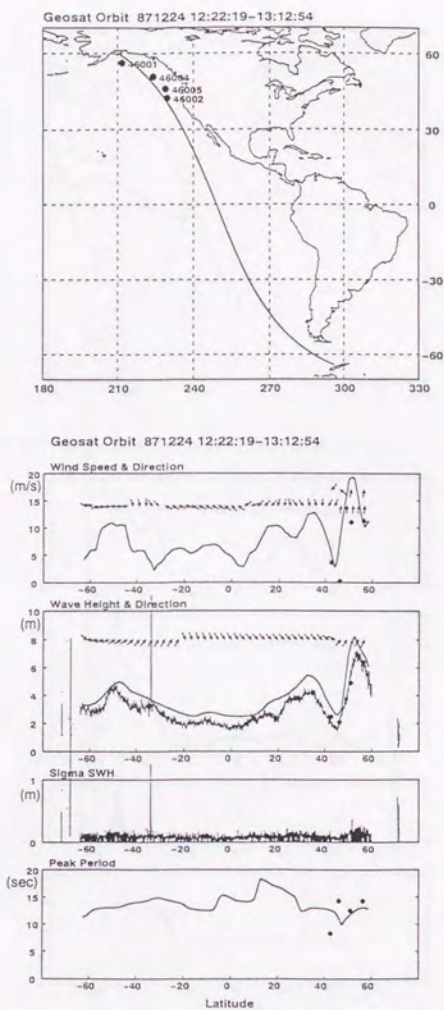


Figure 4.40 GEOSAT orbit (upper) and the comparison of GEOSAT data (thick line) with the model results (thin line) at 1987 12/24 12:22-13:12 (lower). Circles denote location and data of NOAA buoys.

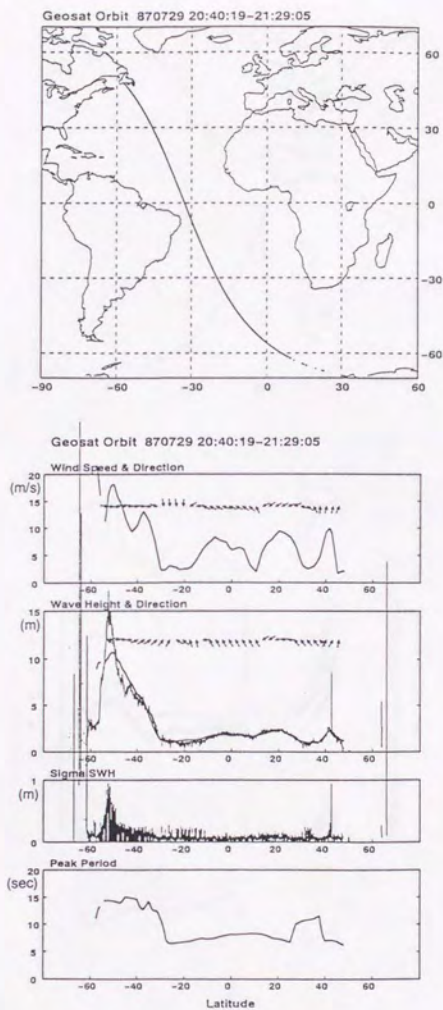


Figure 4.41 Same as Figure 4.40, but for 1987 7/29 20:40-21:29.

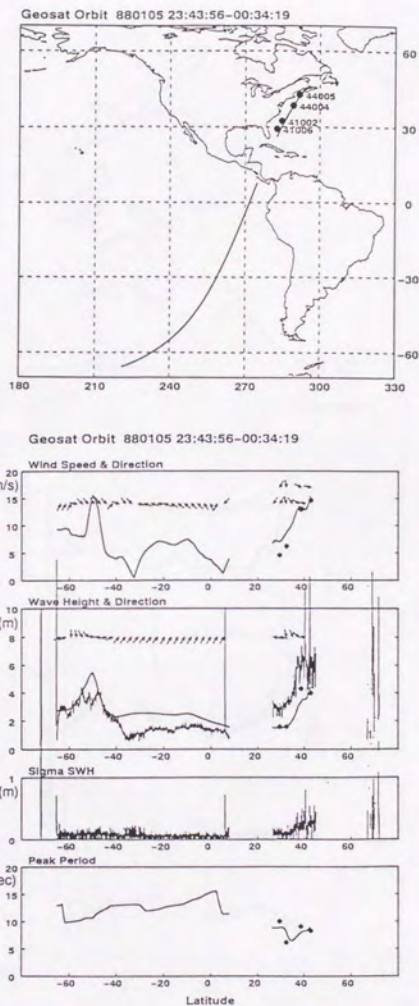


Figure 4.42 Same as Figure 4.40, but for 1988 1/5 23:43:00:34.

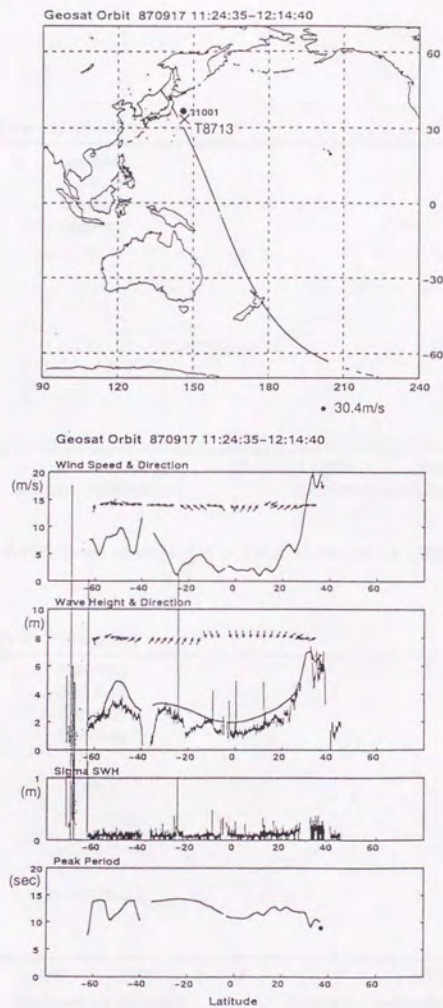


Figure 4.43 Same as Figure 4.40, but for 1987 9/17 11:24-12:14.

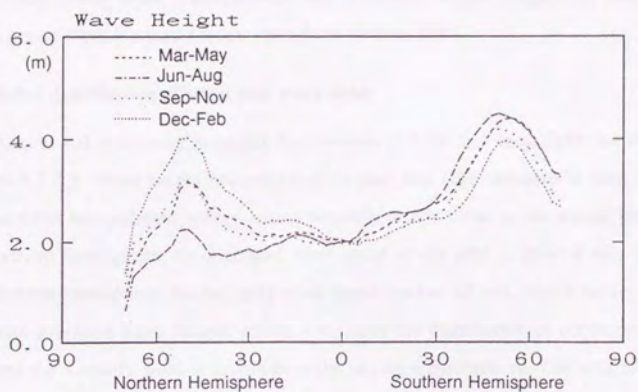


Figure 4.44 Zonal mean wave height of JWA3G model for 1988.

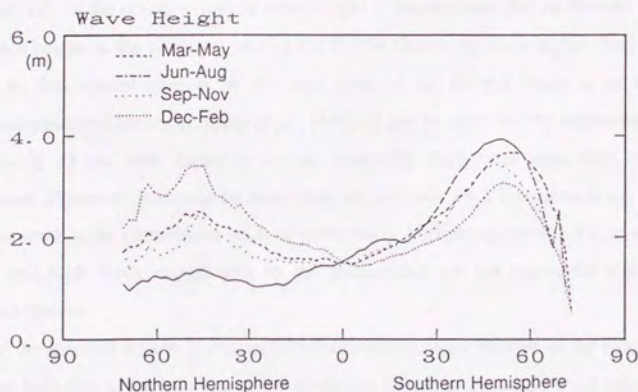


Figure 4.45 Same as Figure 4.44, but for GEOSAT data for 1988.

5. Global ocean wave characteristics

Global ocean wave characteristics are described in this chapter by means of a global ocean wave hindcast for ten years from 1980 to 1989.

5.1 Global distribution of wind and wave fields

Annual and seasonally averaged distributions of wind and wave fields are shown in Figures 5.1-5.5. Wave height becomes high in mid- and high-latitudes of both northern and southern hemispheres, where strong westerly winds blow in the winter season. In the northern hemisphere, the averaged wind speed in the area is about 8 m/s, while in the southern hemisphere, the westerly wind speed reaches 10 m/s, which causes a storm area with averaged wave heights above 4 m, since the distribution of continents which intercept the westerly wind is less than in the northern hemisphere. The area of highest waves in the whole ocean is in the Antarctic Sea at about 50 degrees latitude, to the south of the Indian Ocean. In the north Pacific and north Atlantic Oceans, the distribution of wave height on the west side is different from that on the east side. On the west side of the ocean, averaged wave height is smaller than that on the east side. So the wave height in the northeast part of the Pacific Ocean becomes higher than in other areas, so that coastal erosion on the west coast of the United States is an essential environmental problem (*e.g.*, Earle *et al.*, 1984). It can be seen that the northwest part of the Pacific Ocean near Japan is not an especially high-wave area from a global viewpoint. However, it should be noted that the grid size of 2.5 degrees is too large to express small-scale phenomena such as typhoons or hurricanes, so that the strong wind fields and high wave heights due to the phenomena are not expressed well in the hindcast results.

In the summer season in the northern hemisphere, wave heights in the Arabian Sea become high due to the blowing of the monsoon. Since the averaged wind speed in the area exceeds 10 m/s, the averaged wave height reaches more than 4 m. It is well known among seafarers that the sea state of the Arabian Sea becomes severe in summer, and ships going in to the Red Sea navigate northward along the east coast of Africa in order to avoid the high-wave area due to the monsoon. This experimental knowledge can be

clarified by means of the wave hindcast results.

In the spring season in the northern hemisphere, wave heights in the north Pacific Ocean are higher than those of the north Atlantic Ocean, while in winter, the situation is reversed. Averaged wave heights in the north Atlantic Ocean reach about 5.5 m in winter. The area of highest wave heights in the north Pacific Ocean is located at latitude 40-50 degrees, south of Alaska, while that in the north Atlantic Ocean is located at latitude 50-60 degrees, south of Iceland. Since both areas are close to the great circle path which connects principal cities on the continents, it is necessary to understand the ocean wave characteristics in the area in order to prevent disasters at sea.

Figure 5.6 shows the annual mean wind speed and wave height in the north Pacific Ocean by means of the statistics of data observed by ships (Shipbuilding Research Association of Japan, 1980). By comparing Figure 5.6 with Figure 5.1, the following results are obtained. The maximum wind speed of 17.9 knots (about 9.2 m/s) near latitude 50 degrees almost agrees with the distribution of wind speeds exceeding 9 m/s in the model result (Figure 5.1). However the wind speed at lower latitudes (0-20 degrees) from ship observations (Figure 5.6) is greater than in the model result. The reason why the wind speed observed by ships is greater than the analyzed wind speed by ECMWF, is that the anemometer height on the ships is much higher than 10 m. On the other hand, averaged wave height by ship observation (Figure 5.6) is generally smaller than that of the model (Figure 5.1). The maximum of averaged wave height in the model exceeds 3.5 m, while that in the ship observations is 2.5 m, because high wave conditions are not observed frequently due to the navigation of ships so as to avoid storms. So it is confirmed that the ocean wave hindcast result from JWA3G is more objective than the statistical data by ship observations and becomes a basic data set in place of the observed data by ships.

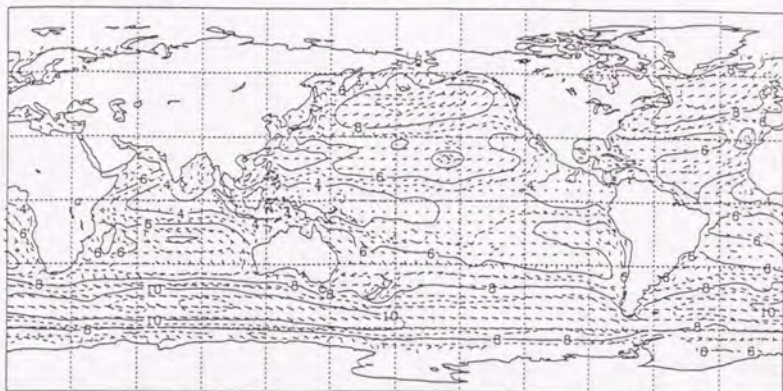
Zonal mean wind speed and wave height from model results are shown in Figure 5.7. There are two peaks at mid-latitudes (40-60 degrees) and low-latitudes (10-20 degrees) in the wind speed distribution. The peak at mid-latitudes corresponds to the westerly jet, while the peak at low-latitudes corresponds to the trade wind. The wind speed becomes maximum in the winter season in each hemisphere except for the peak at mid-latitudes in the southern hemisphere, where the seasonal variation of wind speed is

small. Wave height becomes high generally in winter, but the variation of wave height in the southern hemisphere is also small, as well as that of wind speed. The peak at low-latitudes in wind speed is not clearly seen in the wave height distribution. The reason can be considered to be that the waves generated by trade winds do not become so high, because the wave generation is related to the second power of wind speed rather than to wind speed itself. In mid-latitudes, high wind waves are generated by the strong winds of storms and the waves remain for a long time as a swell component, so that the wave distribution of Figure 5.7 is realized.

Figure 5.8 shows the maximum wind speed and wave height at each grid point during 1980-1989. These distribution of maximum wind speed and wave height are only available from the model results. The maximum wind speed for 10 years appeared in the central area of the north Pacific Ocean at 1983 2/7 00Z with a wind speed of 44.2 m/s and direction of 276 degrees. The maximum wave height for 10 years appeared in the Antarctic Sea off the southwest of Australia at 1980 3/31 00Z with a wave height of 25.8 m and period of 18.8 s. The maximum wave height near Japan is about 12 m, but the value is considered to be lower than the observed data. It can be considered that very high wave heights due to typhoons are not expressed well, because the grid size of 2.5 degrees is so coarse that the analyzed wind field can not represent the typhoon well.

Averaged Wind Speed & Direction

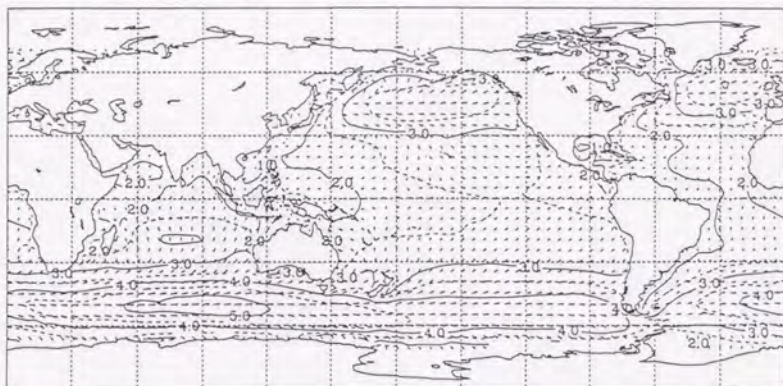
1980-89 Annual



CONTOUR FROM 0 TO 20 BY 1

Averaged Wave Height & Direction

1980-89 Annual

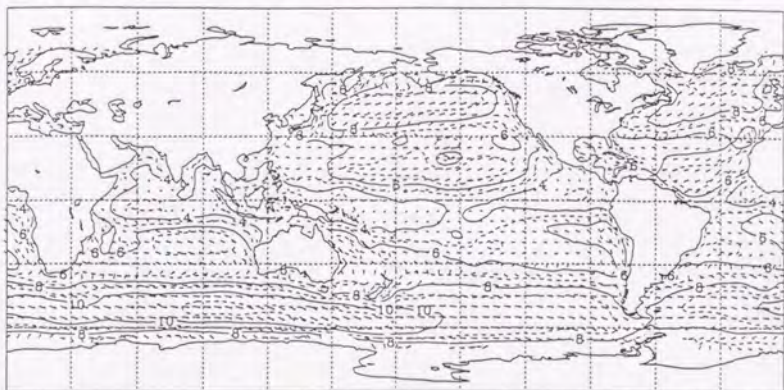


CONTOUR FROM 0 TO 10 BY .5

Figure 5.1 Annual mean wind speed and direction (upper), wave height and direction (lower) for 10 years from 1980 to 1989. Contour interval of wind speed is 1 m/s and 0.5 m for wave height. The length of arrow corresponds to the wind speed and wave height respectively.

Averaged Wind Speed & Direction

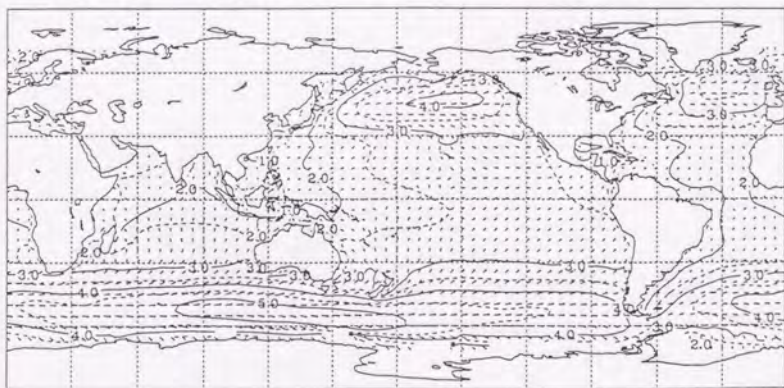
1980-89 Mar-May



CONTOUR FROM 0 TO 20 BY 1

Averaged Wave Height & Direction

1980-89 Mar-May

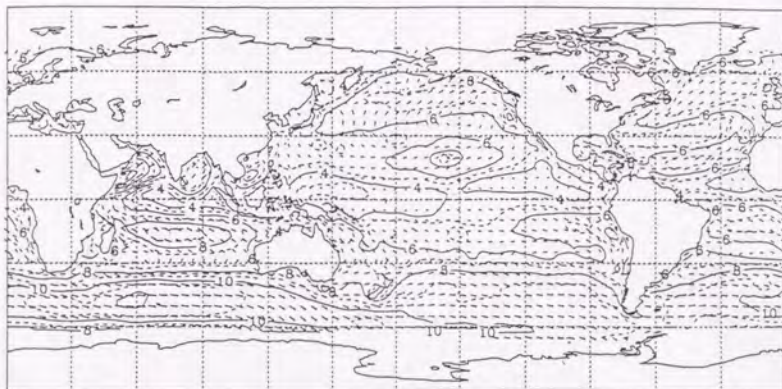


CONTOUR FROM 0 TO 10 BY .5

Figure 5.2 Same as Figure 5.1, but for the seasonal mean for the period from March to May.

Averaged Wind Speed & Direction

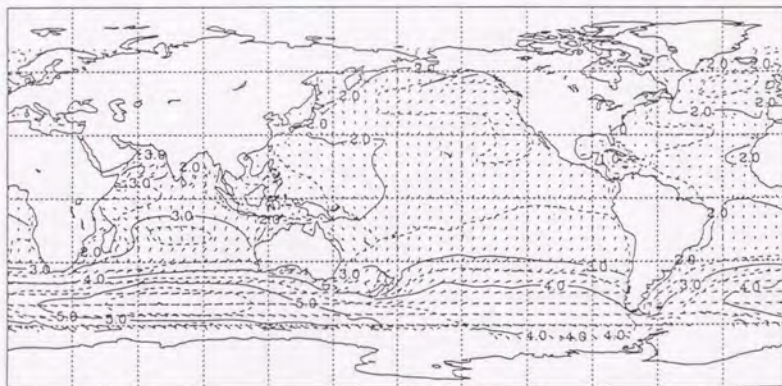
1980-89 Jun-Aug



CONTOUR FROM 0 TO 20 BY 1

Averaged Wave Height & Direction

1980-89 Jun-Aug

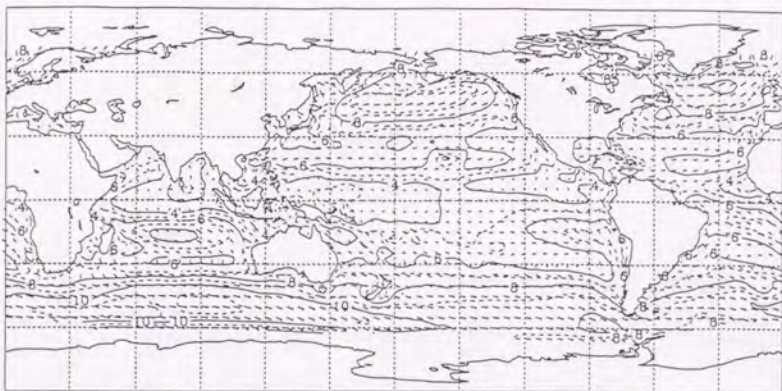


CONTOUR FROM 0 TO 10 BY .5

Figure 5.3 Same as Figure 5.1, but for the seasonal mean for the period from June to August.

Averaged Wind Speed & Direction

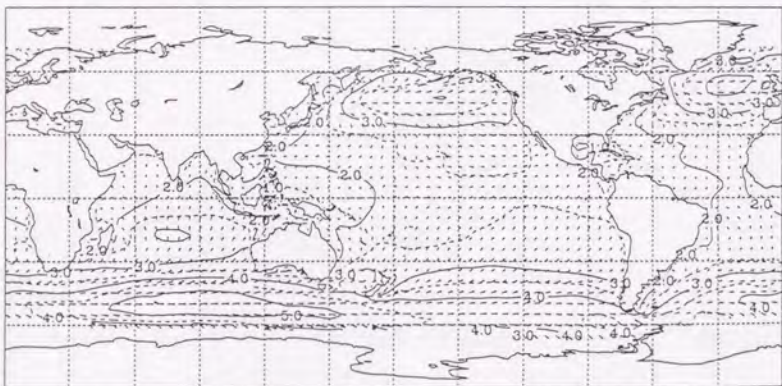
1980-89 Sep-Nov



CONTOUR FROM 0 TO 20 BY 1

Averaged Wave Height & Direction

1980-89 Sep-Nov

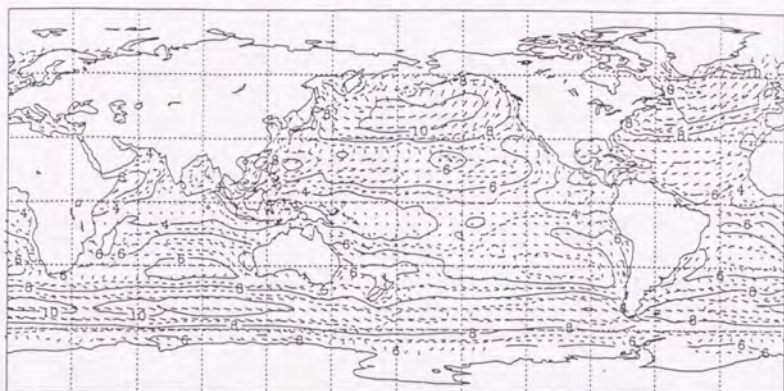


CONTOUR FROM 0 TO 10 BY .5

Figure 5.4 Same as Figure 5.1, but for the seasonal mean for the period from September to November.

Averaged Wind Speed & Direction

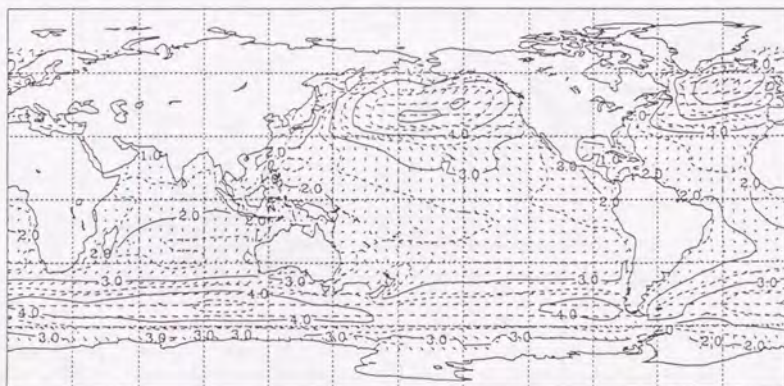
1980-89 Dec-Feb



CONTOUR FROM 0 TO 20 BY 1

Averaged Wave Height & Direction

1980-89 Dec-Feb



CONTOUR FROM 0 TO 10 BY .5

Figure 5.5 Same as Figure 5.1, but for the seasonal mean for the period from December to February.

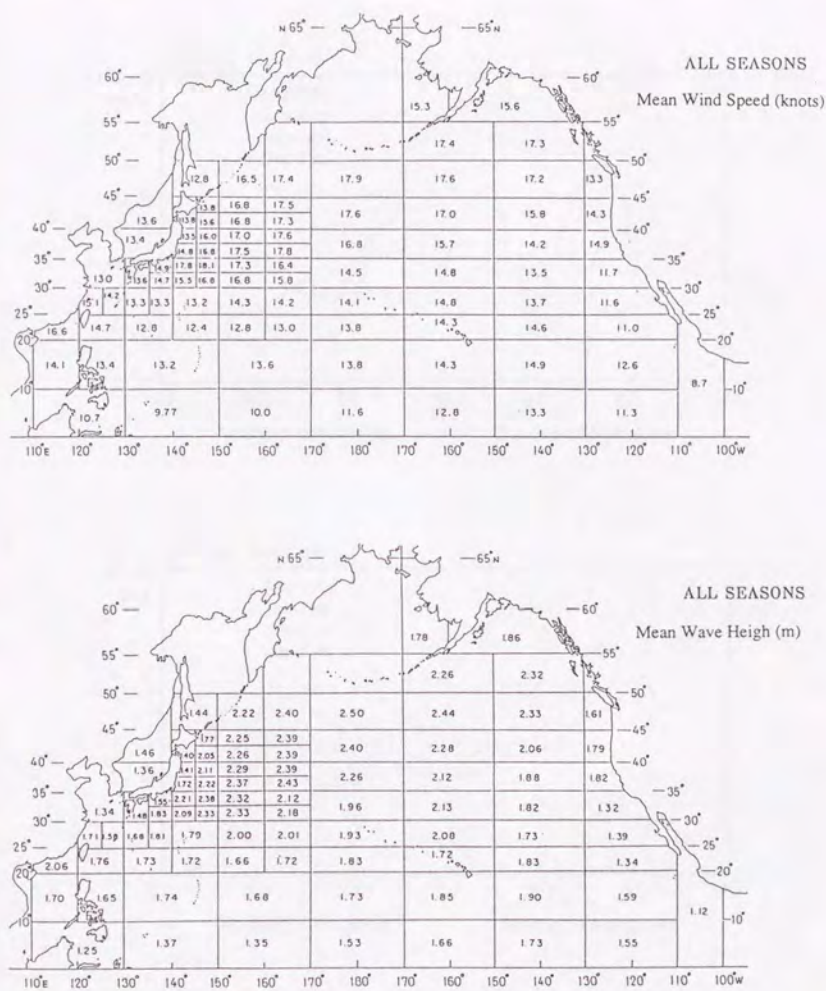


Figure 5.6 Annual mean wind speed (upper), and wave height (lower) in the north Pacific Ocean by using ship observations for the period from 1964 to 1973 (from Shipbuilding Research Association of Japan, 1980).

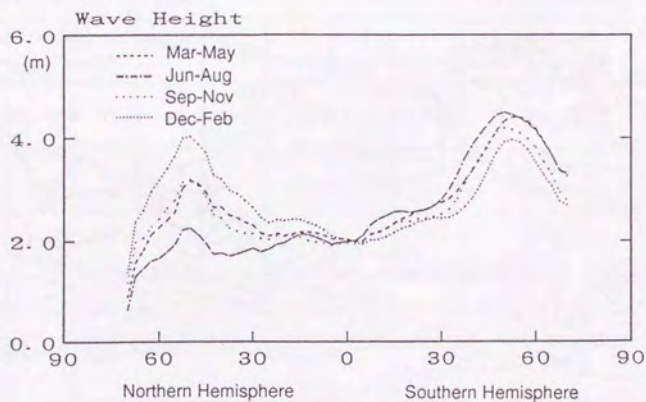
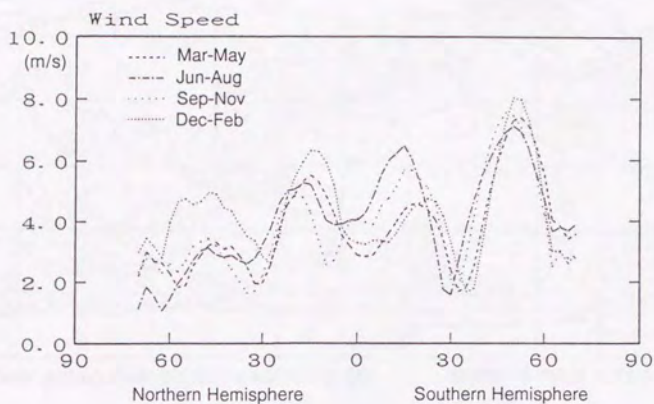


Figure 5.7 Zonal mean wind speed (upper) and wave height (lower) from the ocean wave hindcast results.

Maximum Wind Speed

1980-89 Annual



Maximum: 44.2m/s (1983 2/7 00Z) at (32.5N,162.5E)

CONTOUR FROM 0 TO 50 BY 5

Maximum Wave Height

1980-89 Annual



Maximum: 25.8m (1980 3/31 00Z) at (57.5S,115.0E)

CONTOUR FROM 0 TO 24 BY 3

Figure 5.8 Maximum wind speed (upper) and wave height (lower) at each grid point ($2.5^\circ \times 2.5^\circ$) during 10 years from 1980 to 1989. Contour interval of wind speed is 5 m/s and 3 m for the wave height.

5.2 Characteristics of swell

5.2.1 Swell propagating from the Antarctic Sea

As is obvious from Figure 5.1, there always exist high waves of 4-5 m in wave height around 50 degrees latitude in the Antarctic Sea. There are some reports that the waves generated in this area travel across the Pacific Ocean as swell and can be observed on the coast of California (*e.g.*, Munk *et al.*, 1963). But swell propagation from the Antarctic Sea has not been analyzed in detail, because the observed data by ships is so coarse and continuously observed data in space and time have never been obtained. The problem is solved by applying ocean wave hindcast results.

Figure 5.9 shows the variation of wave height and wave period of southerly wave components, which are defined for the summation of all components from 120 degrees to 240 degrees wave direction. The case in August 1983 is typical of swell propagation from the Antarctic Sea as found by the model. The wave, which developed a height of nearly 10 m on 8/13 in the area of latitude 50 degrees south and longitude 180 degrees east, reached the area off California on 8/22, having undergone a decrease in peak wave height. It can also be clearly seen in the figure that a long-period wave with a period of about 20 seconds propagates preceding the appearance of the peak of wave height.

Let us consider the propagation time of the swell. Substituting the period of the swell $T=15$ seconds into the relation of group velocity of deep water $C_g = gT/4\pi \approx 42$ km/h. The distance between grid points (50°S, 180°E) and (30°N, 240°E) is about 96° (10,700 km), so that the propagation time of the swell is about 255 hours. The time 255 hours later from 8/13 00Z corresponds to 8/23 15Z, which almost agrees with the date of the appearance of the wave height peak in Figure 5.9.

Figure 5.10 shows the distribution of the swell from Antarctic Sea and the change of the location of maximum wave height of the swell. The initial wave height of 7.8 m on 8/14 becomes 2.4 m on 8/20, when the swell crosses the equator, and becomes 2 m on 8/23 when the swell reaches the sea off California. The swell distribution, which is represented by the contour line of 90 % of the maximum wave height, becomes broad as the swell propagates, and the swell is distributed to an extent of several thousands of km from Mexico to Vancouver, when the swell reaches California.

By using ocean wave hindcast results, swell propagation from the Antarctic Sea can be analyzed in detail. With respect to the conditions which are necessary to generate the phenomenon, it is necessary that the northeastward wave component becomes high enough. However, the westerly wind is always strong in the Antarctic Sea, and a northeastward wave component can only be generated behind a depression. When the depression is almost stationary, the duration of strong wind becomes so long that the northeastward waves become high. In contrast, in the Atlantic Ocean, although swell propagating northeastward is generated in the Antarctic Sea, the propagation is interrupted by the west coast of Africa. So swell propagation from the Antarctic Sea can not occur in the Atlantic Ocean in the same way as in the Pacific Ocean.

5.2.2 Sea areas where bi-directional waves prevail

In seas where the bi-directional waves prevail, the response of ships to the ocean wave becomes very complicated, and it is considered that disasters at sea occur more frequently in these areas than in areas of no bi-directional waves. Therefore it is necessary to understand the distribution of bi-directional waves for the purposes of the disaster prevention at sea.

Figures 5.11-5.15 show the annual and seasonal mean distribution of the sea areas where bi-directional waves prevail. The term "bi-directional wave" is defined as a wave which satisfies all of the following conditions.

- a) The difference of wave direction between swell and wind wave component is greater than 45 degrees.
- b) The wave height of both swell and wind-wave components is greater than 1 m.

The most frequent area of the annual distribution of bi-directional waves is in the low-latitudes of the south Indian Ocean, where the frequency exceeds 70 %. Subsequently, the frequency is high in the low-latitudes of the north Atlantic Ocean and north Pacific Ocean, and off the coast of Peru in the south Pacific Ocean. All of these areas are located in low-latitudes where the trade wind is always dominant, so that the local wind-wave generated by the easterly trade wind and the swell propagating from storm areas in high-latitudes overlap in the area.

In spring, the frequency of appearance of bi-directional waves reaches 80 % near Hawaii. In summer, the frequency becomes high in the Arabian Sea and off the coast of

California. This is because the local wind waves due to a strong monsoon become high in Arabian Sea, while the frequency of swell from the Antarctic Sea becomes high off the coast of California. In the southern hemisphere, the frequency becomes high in the sea off the coast of Chile during December-February. The reason is that the seasonal southeasterly wind is dominant in the summer, so that local wind waves are developed.

Bi-directional waves near Japan are most frequent in winter. It is remarkable that the frequency exceeds 50 % in the area off the east coast of Honshu, because the area "Nojima-saki oki" was famous a decade ago as the place where many disasters of big vessels occurred. Since the overall length of the big vessels is close to the wave length of the swell, the response to bi-directional waves is expected to be very complicated. So there is a possibility that the sea condition of bi-directional waves caused disasters for these vessels.

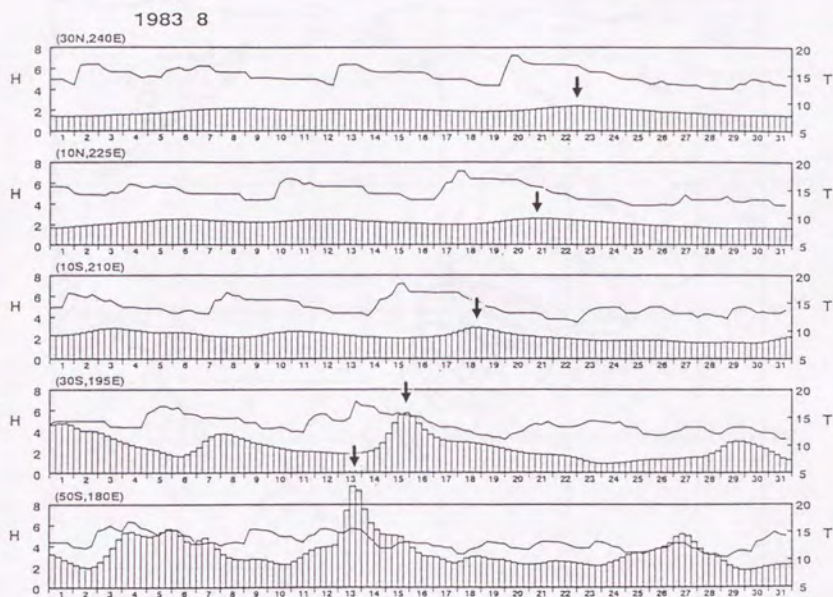


Figure 5.9 Variation of wave height and period for wave components with direction from 120° to 240° in August 1983. Every fifth point is selected on the great-circle path from New Zealand to California. The arrows indicate the peaks of wave height.

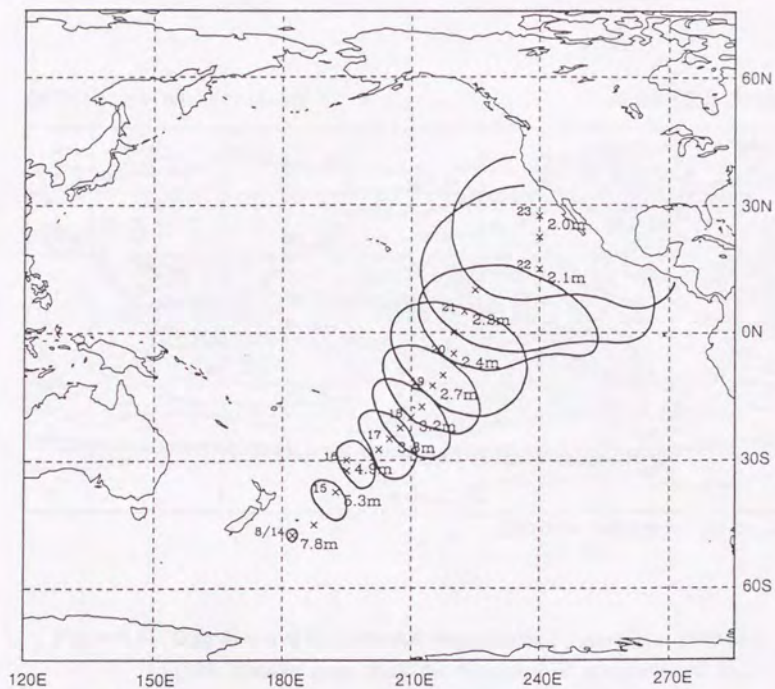
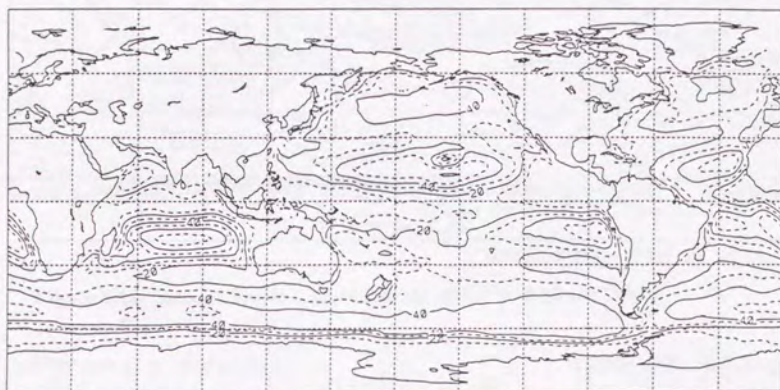


Figure 5.10 Propagation of swell from the Antarctic Sea every 12 hours during 1983 8/14 00Z - 8/23 00Z. Cross marks show the location of maximum wave height of the component with direction from 210° to 240°. Contour lines show the area which exceeds 90 % of the maximum wave height.

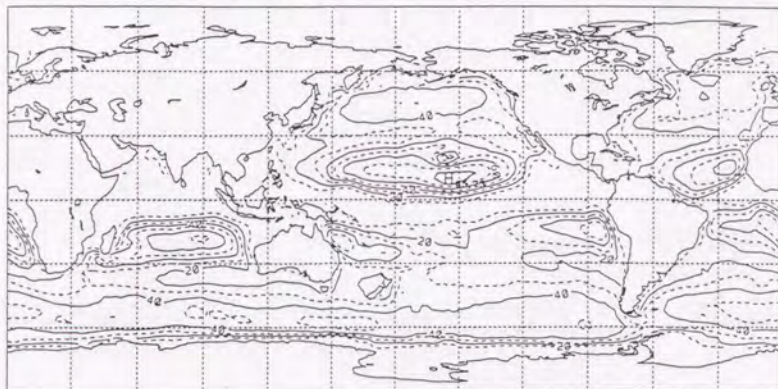


CONTOUR FROM 0 TO 100 BY 10

Figure 5.11 Distribution of bi-directional waves during 10 years from 1980 to 1989. Contour lines show the frequency of appearance of bi-directional waves and the interval is 10 %. Bi-directional waves are defined as waves for which the difference of wave direction between the swell and wind-wave components is above 45° , and both wave heights are above 1 m.

Difference of Direction

1980-89 Mar-May

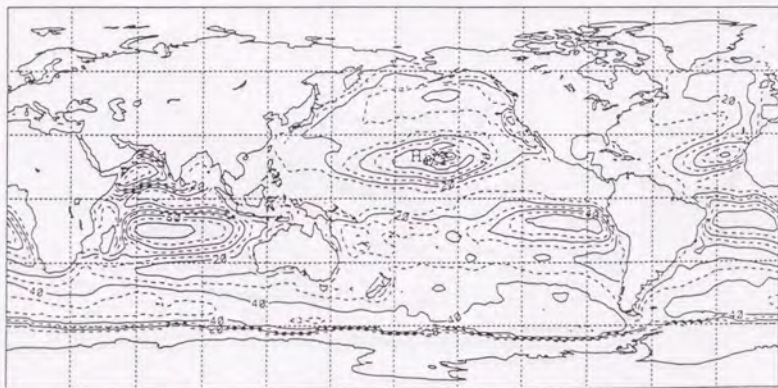


CONTOUR FROM 0 TO 100 BY 10

Figure 5.12 Same as Figure 5.11, but for the period from March to May.

Difference of Direction

1980-89 Jun-Aug

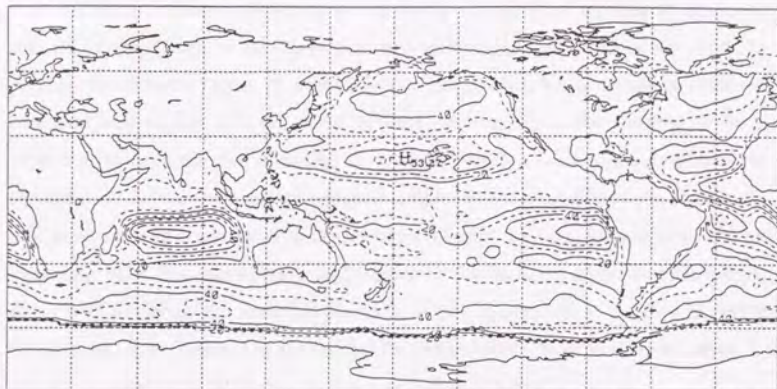


CONTOUR FROM 0 TO 100 BY 10

Figure 5.13 Same as Figure 5.11, but for the period from June to August.

Difference of Direction

1980-89 Sep-Nov

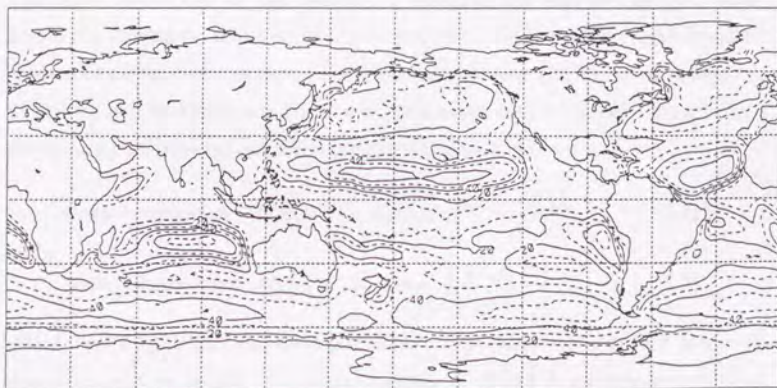


CONTOUR FROM 0 TO 100 BY 10

Figure 5.14 Same as Figure 5.11, but for the period from September to November.

Difference of Direction

1980-89 Dec-Feb



CONTOUR FROM 0 TO 100 BY 10

Figure 5.15 Same as Figure 5.11, but for the period from December to February.

5.3 Probable value of the highest wave height

Statistical estimates of extreme values of wave height and wind speed are basic data for design criteria for structures that must be resistant against waves and wind. As regards coastal wave height, its probable value can be obtained by means of observed data over long periods of time, above 20 years, whereas this is not possible for wave heights in the open sea, due to the lack of observed data. The most essential condition in the statistical analysis is to use an unbiased sample of data taken from a population. On this point, since an ocean wave hindcast gives a series of data in space and time without systematic error, it is reasonable to apply extreme value statistics to the hindcast results. But it is desirable that the statistical period be as long as possible, so the 10-year period of the ocean wave hindcast is not enough for the analysis. Therefore it is necessary to give full consideration to the results of extreme value statistics.

The Petruaskas-Aagaard method, which is applied for the statistical analysis of ocean waves, is adopted as a method of extreme value statistics (Petruaskas and Aagaard, 1970). It is known that the distribution of extreme values approaches some asymptotic distribution as the number of sampled data becomes infinite. Many asymptotic distribution functions have been proposed. The Petruaskas-Aagaard method is based on the Gumbel distribution and Weibull distribution with 7 kinds of parameters, so that the best-fit distribution function to the sampled data is selected among these 8 distributions. The Gumbel and Weibull distributions are expressed as

$$\text{Gumbel distribution: } P(H \leq X) = \exp \left\{ -\exp \left[-\left(\frac{X-B}{A} \right) \right] \right\}, \quad (5.1)$$

$$\text{Weibull distribution: } P(H \leq X) = 1 - \exp \left[-\left(\frac{X-B}{A} \right)^K \right], \quad (5.2)$$

where $P(H \leq X)$ is the cumulative probability which means that the wave height H does not exceed the variable X , and the constants A , B and K are defined as in Table 5.1. For the calculation of the return period, monthly maximum values during 10 years from 1980 to 1989 are sorted in maximum order, and the highest-ranked 40 data are used for extreme value statistics. Figure 5.16 shows an example of fitting the distribution function to the monthly maximum wave height data at (30°N, 150°E). In

most cases of the extreme value statistics of wave height, a Weibull distribution with $K=1.00\sim1.25$ is the best fitting. As shown in the figure, the error bar of 95 % confidence interval becomes greater as the return period becomes greater.

Figure 5.17 shows the distribution of probable wind speed for 20 years and 50 years. The probable wind speed for 50 years is 15-20 m/s in low-latitudes, and 30-40 m/s in mid-latitudes. Although the mean wind speed in mid-latitudes in the southern hemisphere is higher than that in the northern hemisphere (Figure 5.1), probable wind speed in the northern hemisphere is higher than in the southern hemisphere. The proportion of the area where the probable wind speed exceeds 30 m/s is greater in the north Pacific and Atlantic Oceans than in the Antarctic Sea. So it can be considered that the frequency of appearance of extremely developed storms is higher in the northern hemisphere than in the southern hemisphere. Around Japan, the probable wind speed for 50 years is about 30m/s, which can be considered as an underestimated value. The reason is that the strong wind in a typhoon is not expressed well in the analyzed wind data at 2.5-degree grid interval by ECMWF.

Figure 5.18 shows the distribution of probable wave height for 20 years and 50 years. From Figure 5.8, the maximum wave height during 10 years is 25.8 m in the south Indian Ocean, while the probable wave height for 50 years is 27.3 m in the Antarctic Sea near Australia, which is located 10 degrees eastward from the point where the maximum wave height appeared. The distribution of probable wave height has a maximum value at mid-latitudes in both northern and southern hemispheres. Probable wave height in the Antarctic Sea is about 15-18 m, while that of the north Pacific and Atlantic Oceans is above 18 m, which shows an opposite tendency to that of the averaged wave height (Figure 5.1). The reason is considered to be the same as the distribution of probable wind speed. That is to say, in the Antarctic Sea, a strong wind always blows during the whole year so that the averaged wave height never becomes small, while in the north Pacific and Atlantic Oceans, although the averaged wave height becomes small in summer, when the storms are developed in winter, extremely high wave heights occur.

If the period of the ocean wave hindcast becomes longer as wind data accumulate, the extreme value statistics of wind speed and wave height will be more reliable.

Table 5.1 Parameters for Gumbel and Weibull distributions.

Distribution	A	B
Gumbel	0.44	0.12
Weibull($K=0.75$)	0.54	0.64
Weibull($K=0.85$)	0.51	0.59
Weibull($K=1.00$)	0.48	0.53
Weibull($K=1.10$)	0.46	0.50
Weibull($K=1.25$)	0.44	0.47
Weibull($K=1.50$)	0.42	0.42
Weibull($K=2.00$)	0.39	0.37

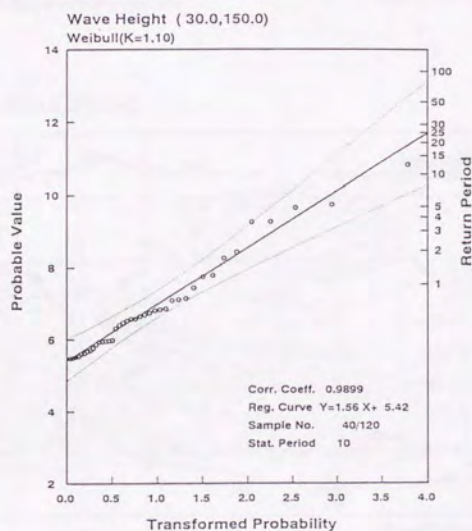


Figure 5.16 An example of fitting the Weibull distribution function to the monthly maximum wave height at (30°N, 150°E). Solid line shows the regression curve and dotted lines show the 95 % confidence interval.

Probable Wind Speed

RP=20



Maximum: 39.1m/s at (35.0N,180.0E)

CONTOUR FROM 0 TO 60 BY 5

Probable Wind Speed

RP=50



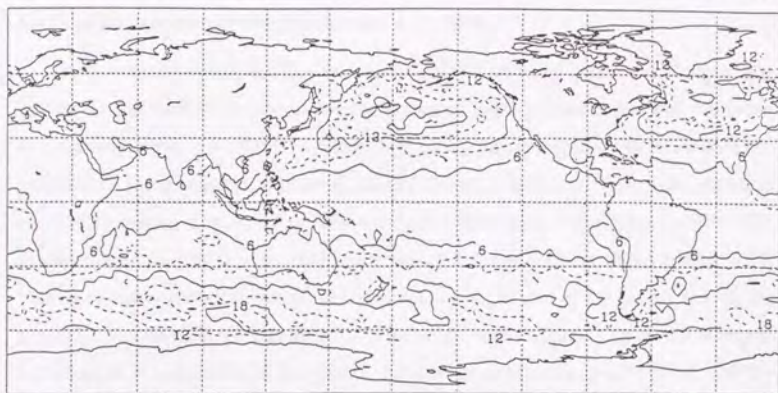
Maximum: 43.5m/s at (32.5N,182.5E)

CONTOUR FROM 0 TO 60 BY 5

Figure 5.17 Probable wind speed for the return period of 20 years (upper) and 50 years (lower). Contour interval is 5 m/s.

Probable Wave Height

RP=20

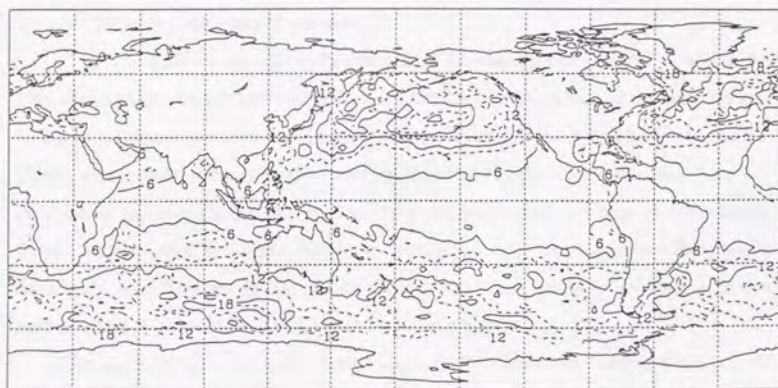


Maximum: 23.4m at (55.0S,115.0E)

CONTOUR FROM 0 TO 30 BY 3

Probable Wave Height

RP=50



Maximum: 27.3m at (55.0S,115.0E)

CONTOUR FROM 0 TO 30 BY 3

Figure 5.18 Probable wave height for the return period of 20 years (upper) and 50 years (lower). Contour interval is 3 m.

5.4 Decadal variation of the global ocean wave field

It was already mentioned that the accuracy of the analyzed wind field changes year by year so that careful considerations are needed in order to discuss decadal variations of the global ocean wave field. However, it is a very interesting study to investigate the variation of wave height in relation to climate change. Figure 5.19 shows the variation of monthly averaged wave height at some typical grid points from 1980 to 1989. The averaged wave height is increasing at the rate of 0.6 cm per year at the point (30°N, 150°E) in the west Pacific Ocean, while decreasing at the rate of 6.6 cm per year at the point (50°N, 210°E) in the east Pacific Ocean. In the north Atlantic Ocean, the averaged wave height is decreasing at the rate of 2.2 cm per year at the point (50°N, 330°E), while increasing at the rate of 4.1 cm per year at the point (10°N, 55°E) in the Arabian Sea. At the point (50°N, 330°E), the amplitude of variation of the monthly mean wave height increases year by year, namely the highest value becomes higher and the lowest value becomes lower simultaneously. As mentioned above, the decadal variation of wave height varies according to the sea area.

Figure 5.20 shows the global distribution of increase in wave height, in which the total variation of wave height during 10 years is calculated by means of the least-squares fitting of a linear regression curve to the monthly averaged wave height. In the Pacific Ocean, an increase of wave height occurs in the west Pacific Ocean, whereas there is a decrease in the east Pacific Ocean. The same distribution can be seen in the Atlantic Ocean, namely that the wave height is increasing near the Caribbean Sea, while decreasing near Europe. In the Indian Ocean, the wave height is increasing in the northern part of the ocean, while decreasing in the southern part.

The variation of wave height near Japan can be verified by means of the coastal wave data observed by JMA (Japan Meteorological Agency, 1991b). Figure 5.21 shows the variation of monthly mean wave height at the coastal wave observing points which are located in the Pacific Ocean. Coastal waves are observed by means of an ultrasonic wave gauge and the depth of the observing point is 50 m, so that the accuracy of the measurement is considered to be high. As shown in the figure, wave height has been increasing for more than ten years at all the points (Enoshima, Irozaki, Sakihama and Kiyamisaki) with a value of 0.7 - 2.5 cm. This result agrees with the analyzed data

from the ocean wave hindcast. Therefore it can be considered as true that the wave height in the Pacific Ocean near Japan is increasing at a rate of about several cm per year.

Figures 5.22 and 5.23 show the variation of global wave height and wind speed. Globally-averaged wave height is decreasing at the rate of 1.9 cm per year. This tendency of decreasing wave height is the same in both northern and southern hemispheres. But the globally-averaged wind speed is increasing at a rate of 2.6 cm/s per year (Figure 5.23). The reason why the wave height is decreasing in spite of the increase of wind speed can be expressed as follows. It can be assumed that the appearance of high wave height decreases due to the decrease of the strong storms, while the mean circulation becomes strong so that the averaged wind speed increases. In order to confirm the assumption, it will be necessary to study the meteorological data in detail.

It will be of great interest to study the relation between the variation of wave height and other meteorological and oceanographic data, in the sense of investigating the relationship between the variation of the ocean waves, and climate change.

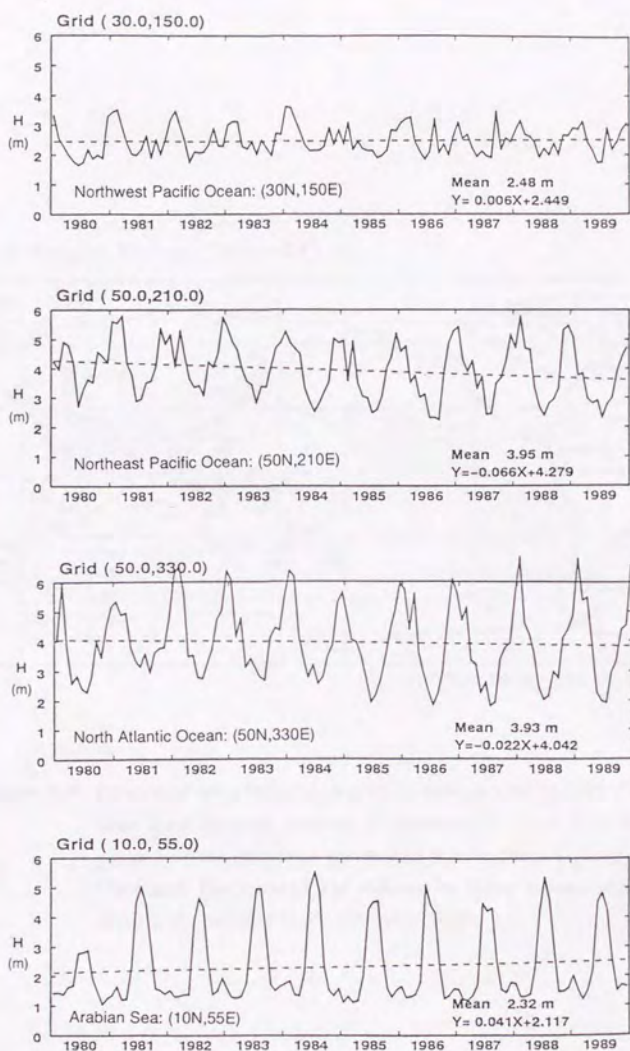


Figure 5.19 Variation of monthly mean wave height from 1980 to 1989. Dashed line shows the linear regression curve $Y = aX + b$, in which the gradient corresponds to an increase in wave height of a m per year.

Wave Height Rising (1980-89)

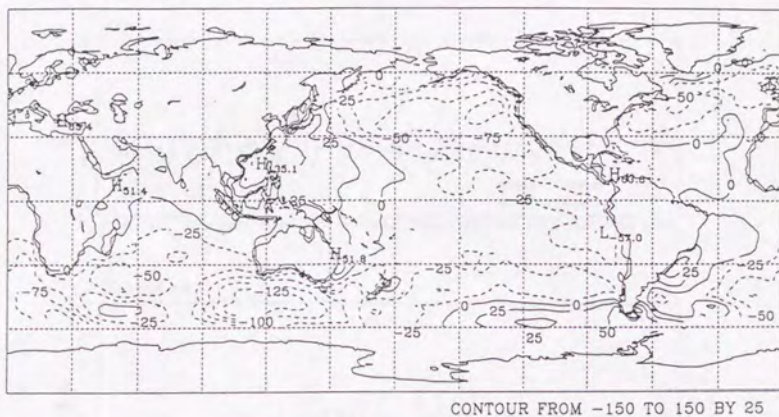


Figure 5.20 Increase of wave height during 10 years from 1980 to 1989. Contour lines show the total increase of wave height. Solid lines indicate positive values (increase) and dashed lines indicate negative values (decrease). The increase was obtained by fitting a linear regression curve to the monthly maximum wave height.

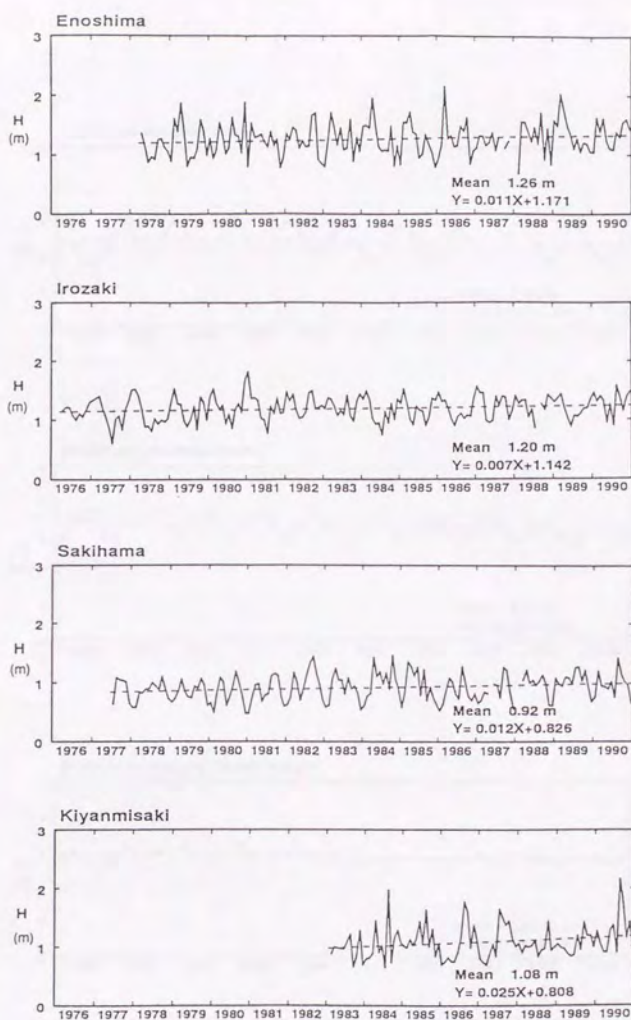


Figure 5.21 Same as Figure 5.19, but for the coastal observation by Japan Meteorological Agency in the Pacific Ocean around Japan.

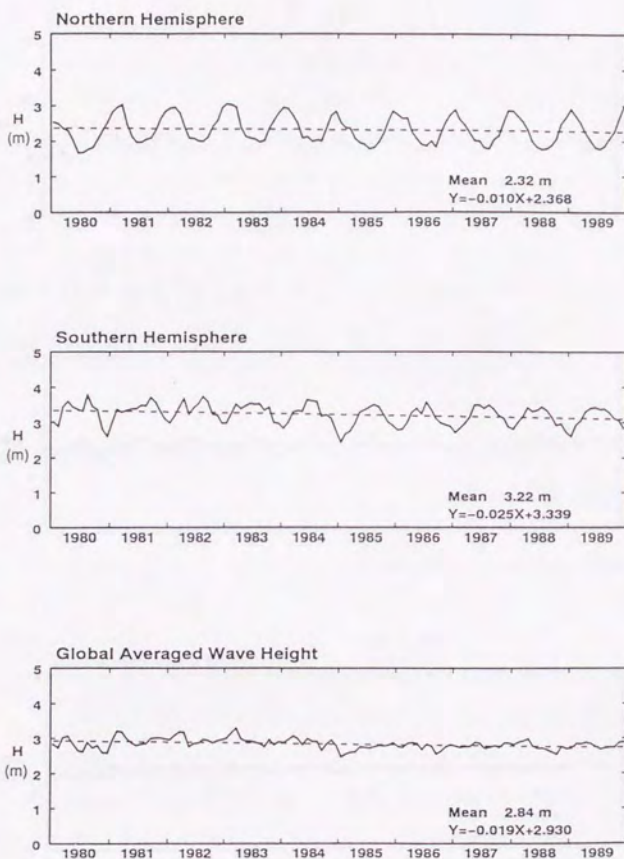


Figure 5.22 Same as Figure 5.19, but for the averaged wave height of the northern hemisphere, southern hemisphere and whole globe.

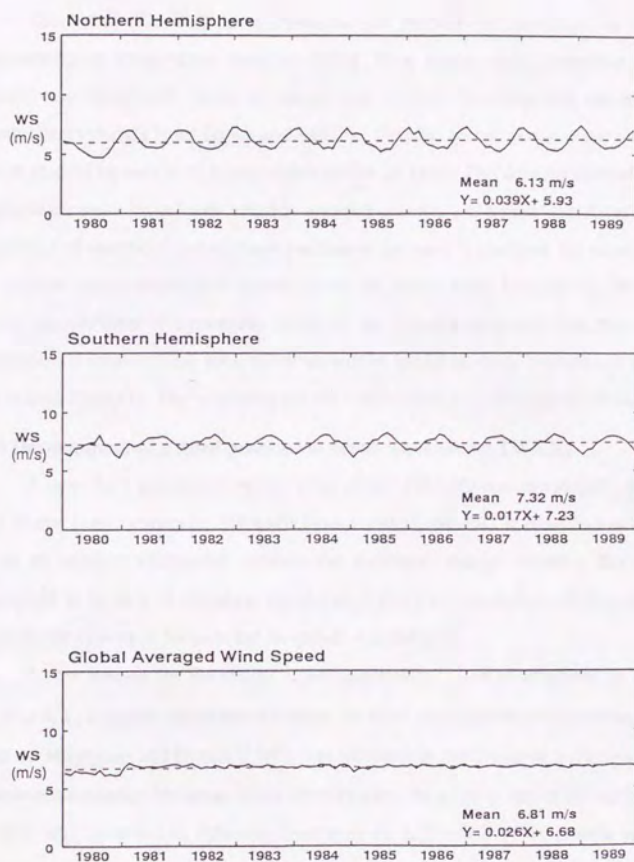


Figure 5.23 Same as Figure 5.22, but for the averaged wind speed. The gradient of the regression curve corresponds to an increase of wind speed (m/s) per year.

6. Concluding discussion

This study has been performed for the purpose of investigating ocean wave characteristics using ocean wave modeling. First, a new third generation ocean wave model was developed. Next, the model was verified by comparing the model results with observed data from buoys and satellite. Finally, global ocean wave characteristics were studied by means of a wave hindcast for 10 years. The development of a new third generation wave model with a highly accurate scheme will be useful not only to raise the accuracy of numerical ocean wave prediction, but also to combine the wave model with a coupled ocean-atmosphere model. Since the ocean wave hindcast by the model will solve the problem of systematic errors in the visually-observed data, the ocean wave statistics by means of the wave hindcast will be useful in many branches of shipbuilding or marine transport. The following are the conclusions and discussions of the study.

(1) Development of a third generation ocean wave model JWA3G

A new third generation ocean wave model JWA3G was developed. According to the model classification by SWAMP Group (1985), JWA3G is classified as a CD model with an explicit calculation scheme for nonlinear energy transfer. The model was designed to be able to calculate the global ocean wave evolution, so that the spherical coordinate system of latitude and longitude was adopted.

A new scheme for the energy input by the wind S_{in} was proposed. In the range of $u_*/c > 0.2$, a typical measurement range for wind-wave tunnel experiments, the growth rate of Mitsuyasu and Honda (1982) was adopted. In the range of $u_*/c \leq 0.2$, a typical measurement range for ocean wave observations, the growth rate of Hsiao and Shemdin (1983) was modified to maintain continuity at $u_*/c = 0.2$. This growth curve almost agrees with Snyder *et al.* (1981) in the range of $u_*/c \leq 0.1$, but in the range of $u_*/c > 0.1$, the growth rate of Snyder *et al.* (1981), which was incorporated into the WAM model, is much smaller than this.

An improved discrete interaction approximation was developed for the calculation of the nonlinear energy transfer S_{nl} due to resonant wave-wave interaction. This new scheme is a modified version of the discrete interaction approximation proposed by

Hasselmann *et al.* (1985). It was found that the accuracy of Hasselmann's scheme for wave spectra with sharp peaks became worse than that for smooth spectra such as the PM spectrum. The improved discrete interaction approximation has succeeded in improving the accuracy of the approximation of nonlinear energy transfer for the sharp spectrum.

A new formula for the energy dissipation S_{ds} was proposed by means of dimensional analysis, on the assumption of energy balance between the energy source functions. It was introduced that the energy dissipation is proportional to ω^3 , where ω is the angular frequency, assuming energy balance in the equilibrium range of the wave spectrum. In addition to that it was found that the dependence of the energy dissipation on the wave slope, which was experimentally determined by Komen *et al.* (1984), was able to be determined on the basis of the 3/2 power law between wave height and period from Toba (1972). Therefore it became clear that the three source functions S_{in} , S_{nl} and S_{ds} had to be a consistent combination with each other. Although the essential meaning of the third generation wave model is to remove the restriction on development of the wave spectrum, it is found that the experimental 3/2 power law was implicitly incorporated in the model.

As regards the finite difference scheme of energy propagation, a new Hybrid Upstream scheme was proposed. For a positive definite value such as wave energy, an upstream scheme is appropriate in order to avoid the generation of negative energy. But the first order forward upstream scheme, which was widely applied in old wave models, has the weak point that the computational diffusion becomes too large. The Hybrid Upstream scheme solved this problem and has a high accuracy, since a third-order upstream scheme was adopted as a corrector of the value predicted by the first-order forward upstream scheme. The accuracy was verified by a simple propagation test of wave energy.

In order to study the basic characteristics of JWA3G, the evolution of the wave field was tested in an idealized rectangular sea with the uniform wind conditions. As a result of the experiment, it was found that the wave spectrum was growing in proportion to f^{-4} while keeping its self-similarity structure; that the overshoot phenomenon was

reproduced; and that the directional distribution of wave energy almost agreed with the observed result from Mitsuyasu *et al.* (1975). The distribution near the spectral peak became narrow, while that in the high-frequency range became broad. From the comparison of fetch- and duration-limited wave growth with other models in the SWAMP (1985) study, it became clear that JWA3G gave valid results that satisfy the $3/2$ power law. But wave growth in short fetch was a little greater than in the SWAMP models. This phenomenon was considered to be due to the insufficiency of the accuracy of the nonlinear energy transfer S_{nl} . So it was concluded that a more accurate scheme for S_{nl} was needed to improve the model.

(2) Verification of the JWA3G model

The accuracy of the JWA3G model was verified using ocean wave hindcast results for 10 years from 1980 to 1989, by comparing with observed data from NOAA buoys and the GEOSAT satellite.

The accuracy of the analyzed sea surface wind data by ECMWF (grid size of 2.5 degrees and time interval of 12 hours), which was used as the forcing term in the wave model, was becoming higher year by year, and the RMS error of wind speed in 1989 became small with the value of about 1 m/s. This is due to an improvement of the objective analysis model of ECMWF. So it should be noted that the accuracy of the calculated wave field using this wind changes year by year. As regards the objective analysis of ECMWF, a re-analysis project for the period 1979-1993 with a resolution of 1 degree interval has already started, so that equally-accurate surface wind data will be available for the ocean wave hindcast.

As a result from case studies of north Pacific Ocean storms, it was found that JWA3G had a better accuracy than the old wave models in case of a sudden change of wind field and a decrease in wave height. When the wind speed increases suddenly, it can be considered that the increase of wave height comes from not only the energy input by the wind, but also from nonlinear energy transfer between the existing wave components and the newly generated wind-wave components. So the merit of the improved discrete approximation scheme of S_{nl} was shown remarkably by this result. The shape of the wave spectrum in the model almost agreed with that observed by

NOAA buoys. However, a small spectral peak at high frequency due to the local wind was not reproduced well. Therefore the accuracy of wave period was lower than that of wave height.

In the case of 1988 4/15-16, a very long-period wave of more than 20 seconds was observed in north Pacific Ocean buoys, which was not calculated by the model. The propagation speed of the wave packet was analyzed to be about 60 km/h, which almost agreed with the moving speed of the storm. Since the storm developed rapidly over 12 hours, it is probable that the phenomenon was generated by the traveling force due to the sudden change of atmospheric pressure.

As a result from the comparison with NOAA and JMA buoy data, the accuracy of wave height was found to be 0.7-0.9 m in RMS error and 0.65-0.85 in correlation coefficient. The accuracy of wave period was less than that of wave height. In the north Pacific Ocean, the bias error was remarkable (especially before 1985), whereas it was not in the north Atlantic Ocean. The reason was considered to be the lack of accuracy of the analyzed wind field and the long life of the swell component of the model. The energy dissipation in the model was determined on the basis of energy balance in the equilibrium range of the spectrum. However, it was extrapolated to the lower frequency range. So the energy dissipation of swell components has less physical basis, and the life time of the swell became long. This is a weak point of JWA3G for the present and it needs to be improved by considering experimental and theoretical studies on the interactions between swell and other factors.

A comparison with GEOSAT data was also performed. It was found that the change of wave height in the meridional direction was expressed well by the model. But the bias error of wave height in the model was still remarkable in the Pacific Ocean. From the comparison of zonal mean wave height in the model with that in the GEOSAT data, both of seasonal change of wave height agrees well. But in the northern hemisphere, there were some differences between model results and satellite data. It is possible that the accuracy of measuring the wave height by the satellite became worse when the swell and wind-wave components were overlapping and the accuracy of the analyzed wind field by ECMWF was not enough.

(3) Global ocean wave characteristics

From the considerations of global ocean wave characteristics by means of the wave hindcast results for 10 years, new ocean wave characteristics, which were never understood from visually-observed data, became clear.

As regards the global ocean wave distribution, it was found that the highest wave height area in the whole globe was in the Antarctic Sea south of the Indian Ocean and the averaged wave height exceeded 4 m. It also became clear that the averaged wave height in the north Pacific and north Atlantic Oceans was higher in the west part than in the east part. In the sea area near Japan, averaged wave height was not so high from a global viewpoint, but it must be noted that the strong wind field and high wave heights due to the typhoon was not expressed well in the grid size of 2.5 degrees. In the summer season of the northern hemisphere, wave heights in the Arabian Sea became high due to the monsoon, and the averaged wave height exceeds 4 m. The maximum wave height during 10 years from 1980 to 1989 was 25.8 m which occurred in the Antarctic Sea, south of the Indian Ocean.

As a result of swell analysis, the propagation of swell from the Antarctic Sea to the coast off California was clearly shown. The propagation time of the swell was almost 10 days. When the swell reached the coast of California, it was distributed over several thousands of km from Mexico to Vancouver. The distribution of sea areas where bi-directional waves were prevailing was also investigated. The frequency of the appearance of bi-directional waves became high in the low-latitudes of the northern and southern hemispheres. It was because the local wind waves generated by the trade winds and swell coming from high latitudes were overlapping in these areas. It was also found that the frequency of bi-directional waves near Japan exceeded 50 % in winter. So there was a possibility that the complicated sea conditions in this area caused the disasters of "Nojima-saki oki".

Probable wave height was obtained for return periods of 20 years and 50 years. The maximum value of probable wave height which is expected to occur once in 50 years, is 27.3 m in the Antarctic Sea near Australia. The distribution was found to be greater in the northern hemisphere than in the southern hemisphere.

As a result of the analysis of decadal variation of wave height, it was found that the wave height was decreasing at a rate of 1.9 cm per year, but the tendency varied with location. The area where the wave height was increasing was both in the west part of the Pacific and Atlantic Oceans and the north part of the Indian Ocean. The increase of wave height near Japan was confirmed by means of observed coastal wave data by Japan Meteorological Agency. However, the accuracy of analyzed wind data changed year by year, and a further analysis on the variation of wave height is needed in relation to climate change.

Appendix A. Energy transport equation in the spherical coordinate

The general energy transport equation with respect to the four dimensional phase space $(f, \theta, \phi, \lambda)$, where f is the frequency, θ the direction, ϕ the latitude and λ is the longitude, can be expressed as

$$\frac{\partial \hat{F}}{\partial t} + \frac{\partial}{\partial \phi}(\dot{\phi} \hat{F}) + \frac{\partial}{\partial \lambda}(\dot{\lambda} \hat{F}) + \frac{\partial}{\partial \theta}(\dot{\theta} \hat{F}) = \hat{S}, \quad (\text{A.1})$$

where $\hat{F}(f, \theta, \phi, \lambda)$ is the spectral density and \hat{S} is the energy source function. \hat{F} is related to the normal spectral density $F(f, \theta, x, y)$ in the Cartesian coordinate through the relation

$$\iint \hat{F} d\phi d\lambda = \iint F dx dy. \quad (\text{A.2})$$

The local Cartesian element $dx dy$ is expressed by using spherical coordinate as

$$dx dy = R^2 \cos \phi d\phi d\lambda, \quad (\text{A.3})$$

where R is the radius of the earth. Substitution of (A.3) into (A.2) gives

$$\hat{F} = F R^2 \cos \phi. \quad (\text{A.4})$$

From the same consideration, the relation

$$\hat{S} = S R^2 \cos \phi, \quad (\text{A.5})$$

is obtained. Substituting (A.4) and (A.5) into (A.1) yields the energy transport equation in the spherical coordinate:

$$\frac{\partial F}{\partial t} + \frac{1}{\cos \phi} \frac{\partial}{\partial \phi}(\dot{\phi} \cos \phi \cdot F) + \frac{\partial}{\partial \lambda}(\dot{\lambda} \cdot F) + \frac{\partial}{\partial \theta}(\dot{\theta} \cdot F) = S. \quad (\text{A.6})$$

Appendix B. Group velocity in the spherical coordinate

The rate of change of the position and propagate direction of a wave packet traveling along a great circle path can be obtained as follows. The northward and eastward components of group velocity C_g with respect to the propagate direction θ is expressed as (cf. Figure B.1)

$$\begin{cases} \text{northward component: } C_g \cos \theta, \\ \text{eastward component: } C_g \sin \theta. \end{cases} \quad (\text{B.1})$$

The each component of group velocity can be written by using angular velocity with respect to latitude ϕ and longitude λ as

$$\begin{cases} R\dot{\phi} = C_g \cos \theta, \\ (R \cos \phi)\dot{\lambda} = C_g \sin \theta, \end{cases} \quad (\text{B.2})$$

where R is the radius of the earth. Therefore the rate of change of the position $\dot{\phi}$ and $\dot{\lambda}$ are given as

$$\begin{cases} \dot{\phi} = \frac{C_g}{R} \cos \theta, \\ \dot{\lambda} = \frac{C_g \sin \theta}{R \cos \phi}. \end{cases} \quad (\text{B.3})$$

Figure B.2 shows a great circle path, on which point $P(\phi_0, \lambda_0)$ and $Q(\phi_1, \lambda_1)$ are defined. The propagate direction θ_0 of a wave packet which was located at P becomes θ_1 at Q , and the rate of change of the wave direction from P to Q corresponds to $\dot{\theta}$. The application of a spherical trigonometry to the orthogonal spherical triangle $\triangle PO'P'$ and $\triangle QO'Q'$ gives

$$\begin{cases} \tan \theta_0 = \frac{\tan \lambda_0}{\sin \phi_0}, \\ \tan \theta_1 = \frac{\tan \lambda_1}{\sin \phi_1}. \end{cases} \quad (\text{B.4})$$

Substitution of the relation

$$\begin{cases} \phi_1 = \phi_0 + \dot{\phi}\Delta t, \\ \lambda_1 = \lambda_0 + \dot{\lambda}\Delta t, \\ \theta_1 = \theta_0 + \dot{\theta}\Delta t, \end{cases} \quad (\text{B.5})$$

into the second equation of (B.4) yields

$$\dot{\phi}(\tan \theta_0 \cos \phi_0) + \dot{\theta} \sin \phi_0 (1 + \tan^2 \theta_0) - \dot{\lambda}(1 + \sin^2 \phi_0 \tan^2 \theta_0) = 0. \quad (\text{B.6})$$

By using equation (B.3), the rate of change of the propagate direction is given as

$$\dot{\theta} = \frac{C_g}{R} \sin \theta \tan \phi. \quad (\text{B.7})$$

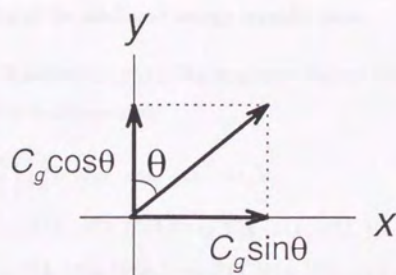


Figure B.1 Components of group velocity in local Cartesian coordinate.

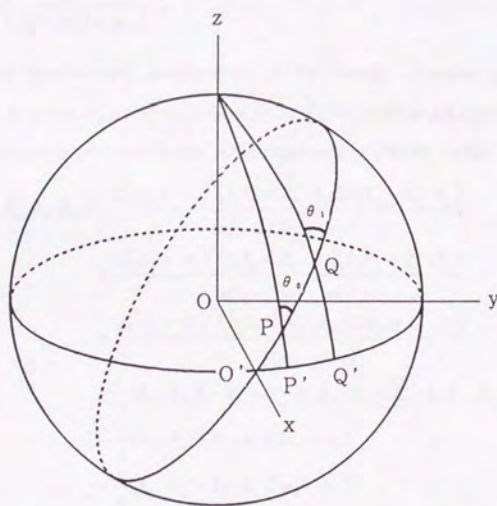


Figure B.2 Great circle path and the change of propagate direction.

Appendix C. Scaling of the nonlinear energy transfer term

According to Hasselmann(1963), The nonlinear energy transfer due to resonant wave-wave interaction is expressed as

$$\begin{aligned} \frac{\partial F(k_4)}{\partial t} = & \iiint a' \delta(\omega_1 + \omega_2 - \omega_3 - \omega_4) \omega_4 \\ & \times [\omega_4 F(k_1) F(k_2) F(k_3) + \omega_3 F(k_1) F(k_2) F(k_4) \\ & - \omega_1 F(k_2) F(k_3) F(k_4) - \omega_2 F(k_1) F(k_3) F(k_4)] dk_1 dk_2, \end{aligned} \quad (C.1)$$

where F is the wave number spectrum, ω the angular frequency and k is the wave number vector which satisfies the relation

$$k_3 = k_1 + k_2 - k_4. \quad (C.2)$$

and

$$a' = \pi \left(\frac{3gD}{2\rho\omega_1\omega_2\omega_3\omega_4} \right)^2. \quad (C.3)$$

Here, g is the gravitational acceleration, ρ the density of water and the transfer coefficient D is given by using equations (4.3), (4.4), (4.9) and (4.10) of Hasselmann (1962). For deep water, the coefficient D is expressed as (Webb, 1978)

$$\begin{aligned} D(k_1, k_2, k_3, k_4) = & \frac{2(w_4 + w_3)^2 (k_3 \cdot k_4 - k_3 \cdot k_4)(k_1 \cdot k_2 - k_1 \cdot k_2)}{w_{4+3}^2 - (w_4 + w_3)^2} \\ & + \frac{2(w_4 - w_1)^2 (k_1 \cdot k_4 + k_1 \cdot k_4)(k_2 \cdot k_3 + k_2 \cdot k_3)}{w_{4-1}^2 - (w_4 - w_1)^2} \\ & + \frac{2(w_4 - w_2)^2 (k_2 \cdot k_4 + k_2 \cdot k_4)(k_1 \cdot k_3 + k_1 \cdot k_3)}{w_{4-2}^2 - (w_4 - w_2)^2} \\ & + \frac{1}{2} (k_3 \cdot k_4 k_1 \cdot k_2 + k_1 \cdot k_4 k_2 \cdot k_3 + k_2 \cdot k_4 k_1 \cdot k_3) \\ & - \frac{1}{4} (k_3 \cdot k_4 + k_1 \cdot k_2)(w_4 + w_3)^4 \\ & + \frac{1}{4} (k_1 \cdot k_4 + k_2 \cdot k_3)(w_4 - w_1)^4 \\ & + \frac{1}{4} (k_2 \cdot k_4 + k_1 \cdot k_3)(w_4 - w_2)^4 \\ & - \frac{5}{2} k_1 k_2 k_3 k_4 \\ & + (w_4 + w_3)^2 (w_4 - w_1)^2 (w_4 - w_2)^2 (k_1 + k_2 + k_3 + k_4), \end{aligned} \quad (C.4)$$

where

$$k_1 = |k_1|, \quad (C.5)$$

$$w_1 = k_1^{1/2}, \quad (C.6)$$

and similarly for $k_2, w_2, etc.$

$$w_{4+3} = |k_4 + k_3|^{1/2}, \quad (C.7)$$

$$w_{4-1} = |k_4 - k_1|^{1/2}, \quad (C.8)$$

$$w_{4-2} = |k_4 - k_2|^{1/2}. \quad (C.9)$$

The nonlinear energy transfer (C.1) is the expression for the wave energy spectrum which is defined in wave number space. For the variance spectrum, which is not multiplied by ρg , the coefficient a' of (C.3) is expressed as

$$a' = \pi \left(\frac{3g^2 D}{2\omega_1 \omega_2 \omega_3 \omega_4} \right)^2. \quad (C.10)$$

The wave number spectrum $F(k)$ is transformed into frequency spectrum $F(\omega, \theta)$ as

$$\begin{aligned} F(k)dk &= F(\omega, \theta)d\omega d\theta, \\ dk &= Jd\omega d\theta, \end{aligned} \quad (C.11)$$

where Jacobian J is given as

$$J = \frac{\partial(k_x, k_y)}{\partial(\omega, \theta)} = \begin{vmatrix} \frac{\partial k_x}{\partial \omega} & \frac{\partial k_x}{\partial \theta} \\ \frac{\partial k_y}{\partial \omega} & \frac{\partial k_y}{\partial \theta} \end{vmatrix} = \frac{2\omega^3}{g^2}. \quad (C.12)$$

Substitution of (C.12) into (C.11) yields

$$F(k) = \frac{g^2}{2\omega^3} F(\omega, \theta). \quad (C.13)$$

From equation (C.4) and (C.10), scaling analysis of the coefficients D and a' by means of g and ω gives

$$\begin{aligned} [D] &\approx k^4 \approx g^{-4} \omega^8, \\ [a'] &\approx k^4 \approx g^{-4} \omega^8. \end{aligned} \quad (C.14)$$

Therefore the nonlinear energy transfer term for the variance spectrum is expressed as

$$[S_{nl}] = \frac{g^2}{\omega^3} \left[\frac{\partial F}{\partial t} \right] \approx [a'] \omega \left(\frac{g^2}{\omega^3} \right)^3 F^3 \left(\frac{\omega^3}{g^2} \right)^2 \omega^2 \approx g^{-4} \omega^{11} F^3. \quad (C.15)$$

References

- Allender, J.H., T.P. Barnett and M. Lybanon, 1985: The DNS model: An improved spectral model for ocean wave prediction. *Ocean Wave Modeling*, The SWAMP Group Ed., Plenum Press, 235-248.
- Al-Zanaidi, M.A. and H.W. Hui, 1984: Turbulent air flow over water waves - A numerical study. *J. Fluid Mech.*, **48**, 225-246.
- Baer, L., 1962: An experiment in numerical forecast of deep water ocean waves. *Lockeed Missile Space Co.*, IMSC-801296.
- Banner, M.L. and I.R. Young, 1994: Modeling spectral dissipation in the evolution of wind waves. Part I: Assessment of existing model performance. *J. Phys. Oceanogr.*, **24**, 1550-1571.
- Barber, N.F. and F. Ursell, 1948: The generation and propagation of ocean waves and swell. I. Wave periods and velocities. *Phil. Trans. Roy. Soc.*, London, **240**, 527-560.
- Barnett, T.P., 1968: On the generation, dissipation and prediction of ocean waves. *J. Geophys. Res.*, **73**, 513-530.
- Barnett, T.P. and J.C. Wilkerson, 1967: On the generation of wind waves as inferred from airborne radar measurements of fetch-limited spectra. *J. Mar. Res.*, **25**, 292-321.
- Barnett, T.P. and A.J. Sutherland, 1968: A note on an overshoot effect in wind-generated waves. *J. Geophys. Res.*, **73**, 6879-6885.
- Boyle, P.J., K.L. Davidson and D.E. Spiel, 1987: Characteristics of over water surface stress during STREX. *Dyn. Atmos. Oceans*, **10**, 343-358.
- Bretschneider, C.L., 1952: The generation and decay of wind waves in deep water. *Trans. A.G.U.*, **33**(3), 381-389.
- Bretschneider, C.L., 1958: Revision in wave forecasting; deep and shallow water. *Proc. 6th Conf. Coastal Eng.*, 30-67.
- Burgers, G.J.H., 1990: A guide to the Neddam wave model. *KNMI Sci. Rep.*, **WR-90-04**.
- Burgers, G.J.H. and V.K. Makin, 1993: Boundary-layer model results for wind-sea growth. *J. Phys. Oceanogr.*, **23**, 372-385.
- Cartwright, D.E. and M.S. Longuet-Higgins, 1956: Statistical distribution of the maxima of random function. *Proc. Roy. Soc. A*, **237**, 212-232.
- Charnock, H., 1955: Wind stress on a water surface. *Quart. J. Roy. Meteor. Soc.*, **81**, 639-640.
- Clancy, R.M., J.E. Kaitala and L.V. Zambresky, 1986: The Fleet Numerical Oceanography Center global spectral ocean wave model. *Bull. Amer. Meteor. Soc.*, **67**, 498-512.
- Darbyshire, J., 1955: An investigation of storm waves in the North Atlantic Ocean. *Proc. Roy. Soc. A*, **230**, 560-569.
- Dobson, E.B., F. Monaldo, J. Goldhirsh and J. Wilkerson, 1987: Validation of Geosat altimeter-derived wind speeds and significant wave heights using buoy data. *Johns Hopkins APL Tech. Dig.*, **8**, 222-223.

- Donelan, M.A., 1982: The dependence of the aerodynamic drag coefficient on wave parameters. *Proc. First Int. Conf. on Meteor. and Air-Sea Interaction of the Coastal Zone*, The Hague, Amer. Meteor. Soc., 381-387.
- Duin, C.A. van and P.A.E.M. Janssen, 1992: An analytic model of the generation of surface gravity waves by turbulent air flow. *J. Fluid Mech.*, **236**, 197-215.
- Earle, M.D., K.A. Bush and G.D. Hamilton, 1984: High-height long-period ocean waves generated by a severe storm in the northeast Pacific ocean during February 1983. *J. Phys. Oceanogr.*, **14**, 1286-1299.
- Ebuchi, N., H. Kawamura and Y. Toba, 1992: Growth of wind waves with fetch observed by the Geosat altimeter in the Japan Sea under winter monsoon. *J. Geophys. Res.*, **97**, 809-819.
- European Centre for Medium-range Weather Forecasts, 1993: *The description of the ECMWF/WCRP Level III-A global atmospheric data archive*, 49pp.
- Ewing, J.A., 1971: A numerical wave prediction method for the North Atlantic ocean. *Dtsch. Hydrogr. Zeit.*, **24**, 241-261.
- Garatt, J.R., 1977: Review of drag coefficients over oceans and continents. *Mon. Wea. Rev.*, **105**, 915-929.
- Gelci, R., H. Cazale and J. Vassale, 1956: Utilisation des diagrammes de propagation à la prévision énergétique de la houle. *Bull. Infor. Comité Central Océanogr. Etude Côtes*, **8**, 170-187.
- Gibson, J.K., P. Kållberg, A. Nomura and S. Uppala, 1994: The ECMWF Re-Analysis (ERA) project - Plans and Current status. *Tenth Inter. Conf. on Interactive Information and Processing Systems for Meteor., Oceanogr. and Hydrology*, in Nashville, USA, 164-167.
- Golding, B., 1983: A wave prediction system for real-time sea state forecasting. *Quart. J. Roy. Meteor. Soc.*, **109**, 393-416.
- Greenwood, J.A., V.J. Cardone and L.M. Lawson, 1985: Intercomparison test version of the SAIL wave model. *Ocean Wave Modeling*, The SWAMP Group Ed., Plenum Press, 221-233.
- Günther, H., W. Rosenthal, T.J. Weare, B.A. Worthington, K. Hasselmann and J.A. Ewing, 1979: A hybrid parametrical wave prediction model. *J. Geophys. Res.*, **84**, 5727-5738.
- Hasselmann, K., 1960: Grundgleichungen der Seegangsvoraussage. *Schiffstechnik*, **7**, 191-195.
- Hasselmann, K., 1962: On the non-linear energy transfer in a gravity-wave spectrum. Part 1. General theory. *J. Fluid Mech.*, **12**, 481-500.
- Hasselmann, K., 1963: On the non-linear energy transfer in a gravity-wave spectrum. Part 3. Evaluation of the energy flux and swell-sea interaction for a Neumann spectrum. *J. Fluid Mech.*, **15**, 385-398.
- Hasselmann, K., 1968: Weak-interaction theory of ocean waves. *Basic developments in fluid dynamics*, M. Holt Ed., New York, **2**, 117-182.

- Hasselmann, K., 1974: On the spectral dissipation of ocean waves due to white capping. *Bound.-Layer Meteor.*, **6**, 107-127.
- Hasselmann, K., T.P. Barnett, E. Bouws, H. Carson, D.E. Cartwright, K. Enke, J.A. Ewing, H. Gienapp, D.E. Hasselmann, P. Kruseman, A. Meertburg, P. Muller, D.J. Olbers, K. Richter, W. Sell and H. Walden, 1973: Measurements of wind-wave growth and swell decay during the Joint North Sea Wave Project (JONSWAP). *Dtsch. Hydrogr. Zeit.*, Suppl. A, **8**(12), 95pp.
- Hasselmann, S. and K. Hasselmann, 1981: A symmetrical method of computing the nonlinear transfer in a gravity-wave spectrum. *Hamb. Geophys. Einzelschriften, Reihe A: Wiss. Abhand.*, **52**, 138pp.
- Hasselmann, S., K. Hasselmann, J.H. Allender and T.P. Barnett, 1985: Computations and parameterizations of the nonlinear energy transfer in a gravity-wave spectrum. Part II: Parameterizations of the nonlinear energy transfer for application in wave models. *J. Phys. Oceanogr.*, **15**, 1378-1391.
- Hogben, N. and F.E. Lumb, 1967: *Ocean Wave Statistics*, National Physical Lab., London, Her Majesty's Stationery Office.
- Hogben, N., N.M.C. Dacunha and G.F. Olliver, 1986: *Global Wave Statistics*, British Maritime Technology.
- Hsiao, S.V. and O.H. Shemdin, 1983: Measurements of wind velocity and pressure with a wave follower during MARSEN. *J. Geophys. Res.*, **88**(C14), 9841-9849.
- Hsu, Y.-J. and A. Arakawa, 1990: Numerical modeling of the atmosphere with an isentropic vertical coordinate. *Mon. Wea. Rev.*, **118**, 1933-1959.
- Inoue, T., 1967: On the growth of the spectrum of a wind generated sea according to a modified Miles-Phillips mechanism and its application to wave forecasting. TR-67-5, *Geophys. Sci. Lab. Rep., New York Univ.*
- Ijima, T., T. Fukushima and T. Matsuo, 1967: On the distribution of wave heights in the typhoon area based on the numerical simulation - Case study of the typhoon over the ocean-. *Proc. Coastal Eng., JSCE*, **14**, 29-38 (in Japanese).
- Isozaki, I., 1974: Ocean wave hindcasting and forecasting, *Rept. Studies on Ocean Waves*. 286-302 (in Japanese).
- Isozaki, I., 1990: *An Introduction to the Ocean Waves*, Japan Weather Association, 276pp (in Japanese).
- Isozaki, I. and T. Uji, 1973: Numerical prediction of ocean wind waves. *Papers in Meteor. and Geophys.*, **24**, 207-231.
- Isozaki, I. and T. Uji, 1974: Numerical model of marine surface winds and its application to the prediction of ocean wind waves. *Papers in Meteor. and Geophys.*, **25**, 197-231.
- Janssen, P.A.E.M., G.J. Komen and W.J.P. de Voort, 1984: An operational coupled hybrid wave prediction model. *J. Geophys. Res.*, **89**(C3), 3635-3654.
- Janssen, P.A.E.M., P. Lionello, M. Reistadt and A. Hollingsworth, 1989: Hindcasts and data assimilation studies with the WAM model during the Seasat period. *J. Geophys. Res.*, **94**, 973-993.

- Japan Meteorological Agency, 1990: *Data from Ocean Data Buoy Stations No.13*, 113pp.
- Japan Meteorological Agency, 1991a: *The Statistical Data of Sea Ice No.2*, 103pp.
- Japan Meteorological Agency, 1991b: *The Report of Sea Waves Observations*, 325pp.
- Joseph, P.S., S.Kawai and Y.Toba, 1981a: Ocean wave prediction by a hybrid model - Combination of single-parameterized wind waves with spectrally treated swells. *Sci. Rep. Tohoku Univ.*, Ser. 5, **28**, 27-45.
- Joseph, P.S., S.Kawai and Y.Toba, 1981b: Prediction of ocean waves based on the single-parameter growth equation of wind waves. II. Introduction of grid method. *J.Oceanogr.Soc.Japan*, **37**, 20-31.
- Kawai, S., 1979: Generation of initial wavelets by instability of a coupled shear flow and their evolution to wind waves. *J.Fluid Mech.*, **93**, 661-703.
- Kawai, S., K.Okada and Y.Toba, 1977: Field data support of three-seconds power law and the $g\mu, \sigma^{-4}$ - spectral form for growing wind waves. *J.Oceanogr.Soc.Japan*, **33**, 137-150.
- Kawai, S., P.S.Joseph and Y.Toba, 1979: Prediction of ocean waves based on the single-parameter growth equation of wind waves. *J.Oceanogr.Soc.Japan*, **35**, 151-167.
- Kinsman, B., 1965: *Wind Waves*, Dover Pub., Inc., New York, 676pp.
- Kitaigorodskii, S.A., 1962: Applications of the theory of similarity to the analysis of wind-generated wave motion as a stochastic process. *Izv.Geophys.Ser.Acad.Sci., USSR*, **1**, 105-117.
- Kitaigorodskii, S.A. and Y.A.Volkov, 1965: On the roughness parameter of the sea surface and the calculation of momentum flux in the near-water layer of the atmosphere. *Izv.Atmos.Ocean.Phys.*, **1**, 973-988.
- Komen, G.J., S.Hasselmann and K.Hasselmann, 1984: On the existence of a fully developed wind-sea spectrum. *J.Phys.Oceanogr.*, **14**, 1271-1285.
- Lamb, H., 1932: *Hydrodynamics*, 6th edn., Cambridge Univ. Press, 738pp.
- Lazanoff, S.M., N.A.Stevenson and V.J.Cardone, 1973: A mediterranean sea wave spectral model. *Technical Note 73-1, Fleet Numerical Oceanogr.Center*, 83pp.
- Lionello, P., H.Gunther and P.A.E.M.Janssen, 1992: Assimilation of altimeter data in a global third-generation wave model. *J.Geophys.Res.*, **97**(C9), 14453-14474.
- Longuet-Higgins, M.S., 1952: On the statistical distribution of the height of sea waves. *J. Mar. Res.*, **11**, 245-266.
- Masuda, A., 1980: Nonlinear energy transfer between wind waves. *J.Phys.Oceanogr.*, **10**, 2082-2093.
- Masuda, A., 1986: Nonlinear energy transfer between random gravity waves. *Wave Dynamics and Radio Probing of the Ocean Surface*, O.M.Phillips and K.Hasselmann Ed., Plenum Press., 41-57.
- Masuda, A. and T.Kusaba, 1987: On the local equilibrium of winds and wind-waves in relation to surface drag. *J.Oceanogr.Soc.Japan*, **43**, 28-36.

- Melville, W.K., 1994: Energy dissipation by breaking waves. *J. Phys. Oceanogr.*, **24**, 2041-2049.
- Miles, J.W., 1957: On the generation of surface waves by shear flows. *J. Fluid Mech.*, **3**, 185-204.
- Miles, J.W., 1960: On the generation of surface waves by turbulent shear flows. *J. Fluid Mech.*, **7**, 469-478.
- Miles, J.W., 1993: Surface-wave generation revisited. *J. Fluid Mech.*, **256**, 427-441.
- Mitsuyasu, H., 1995: *The Physics of the Ocean Waves*, Iwanami Press, 210pp (in Japanese).
- Mitsuyasu, H., F.Tasai, T.Suhara, S.Mizuno, M.Ohkusu, T.Honda and K.Rikiishi, 1975: Observation of the directional spectrum of ocean waves using a cloverleaf buoy. *J. Phys. Oceanogr.*, **5**, 750-760.
- Mitsuyasu, H., F.Tasai, T.Suhara, S.Mizuno, M.Ohkusu, T.Honda and K.Rikiishi, 1980: Observation of the power spectrum of ocean waves using a cloverleaf buoy. *J. Phys. Oceanogr.*, **10**, 286-296.
- Mitsuyasu, H. and T.Honda, 1982: Wind-induced growth of water waves. *J. Fluid Mech.*, **123**, 425-442.
- Mitsuyasu, H. and Y.Yoshida, 1989: Ocean atmosphere interaction on the sea surface when the swell is propagating against the wind. *Rep.Res.Inst.Appl.Mech., Kyushu Univ.*, **68**, 47-71 (in Japanese).
- Munk, W.H., G.R.Miller, F.E.Snodgrass and N.F.Barber, 1963: Directional recording of swell from distant storms. *Phil.Trans.Roy.Soc.London*, **255A**, 505-584.
- Nagata, Y., 1971: Ocean waves. *Lectures in Oceanography III*, 1. Tokai Univ. Press, 1-107 (in Japanese).
- National Oceanic and Atmospheric Administration, 1989: *NDBC data availability summary*, 85pp.
- National Oceanic and Atmospheric Administration, 1990: *Climatic summaries for NDBC buoys and stations update 1*. 454pp.
- National Oceanic and Atmospheric Administration, 1991: *The complete Geosat altimeter GDR handbook*, NOAA manual NOS NGS 7, 79pp.
- National Oceanic and Atmospheric Administration, 1994: *National data buoy center non-directional and directional wave data analysis procedures*. 66pp.
- Neumann, G., 1953: On ocean wave spectra and a new method of forecasting wind-generated sea. *Beach Erosion Board, U.S.Army Corps of Engineers, Tech.Mem. No.43*, 42pp.
- Okada, K., 1994: *A study on a wave prediction in inland sea*. Dr. Thesis, Tohoku Univ., 179pp (in Japanese).
- Petrukas, C. and P.M.Aagaard, 1970: Extrapolation of historical storm data for estimating design wave heights. *Prept. 2nd Offshore Tech. Conf.*, **No.1190**, 409-428.

- Phillips, O.M., 1957: On the generation of waves by turbulent wind. *J. Fluid Mech.*, **2**, 417-445.
- Phillips, O.M., 1958: The equilibrium range in the spectrum of wind-generated waves. *J. Fluid Mech.*, **4**, 426-434.
- Phillips, O.M., 1960: On the dynamics of unsteady gravity waves of finite amplitude, 1, The elementary interactions. *J. Fluid Mech.*, **9**, 193-217.
- Phillips, O.M., 1977: *The Dynamics of the Upper Ocean*. 2nd ed., Cambridge Univ. Press, New York, 336pp.
- Phillips, O.M., 1985: Spectral and statistical properties of the equilibrium range in wind-generated gravity waves. *J. Fluid Mech.*, **156**, 505-531.
- Phillips, O.M. and M.L. Banner, 1974: Wave breaking in the presence of wind drift and swell. *J. Fluid Mech.*, **66**, 625-640.
- Pierson, W.J., G. Neumann and R.W. James, 1955: Practical methods for observing and forecasting ocean waves by means of wave spectra and statistics. *U.S. Navy Hydrogr. Office, Pub. No. 603*, 284pp.
- Pierson, W.J. and L. Moskowitz, 1964: A proposed spectral form for fully developed wind seas based on the similarity theory of S.A. Kitaigorodskii. *J. Geophys. Res.*, **69**, 5181-5190.
- Pierson, W.J., L.J. Tick and L. Baer, 1966: Computer based procedures for preparing global wave forecasts and wind field analysis capable of using wave data obtained by a spacecraft. *Proc. 6th. Naval Hydro. Symp., Washington, D.C.*, 499-533.
- Plant, W.J., 1982: A relationship between wind stress and wave slope. *J. Geophys. Res.*, **87**, 1961-1967.
- Rice, S.O., 1944: Mathematical analysis of random noise. *Reprint in Selected Papers on Noise and Stochastic Processes*, Dover Pub. Inc., 133-294.
- Romeiser, R., 1993: Global validation of the wave model WAM over a one-year period using Geosat wave height data. *J. Geophys. Res.*, **98**(C3), 4713-4726.
- Saïd, F. and A. Druilhet, 1991: Experimental study of the atmospheric marine boundary layer from in-situ aircraft measurements (TOSCANE-T campaign): Variability of boundary conditions and eddy flux parameterization. *Bound.-Layer Meteor.*, **57**, 219-249.
- Sanders, J.W., 1976: A growth-stage scaling model for the wind-driven sea. *Dtsch. Hydrogr. Zeit.*, **29**, 136-161.
- The Shipbuilding Research Association of Japan, 1980: *Winds and waves of the north Pacific Ocean*, 123pp.
- Snyder, R.L. and C.S. Cox, 1966: A field study of the wind generation of ocean waves. *J. Mar. Res.*, **24**, 141-178.
- Snyder, R.L., F.W. Dobson, J.A. Elliott and R.B. Long, 1981: Array measurements of atmospheric pressure fluctuations above surface gravity waves. *J. Fluid Mech.*, **102**, 1-59.

- Suzuki, Y., 1994: On the global ocean wave dataset based on the numerical wave model. *J. Japan Inter. Marine Sci. and Tech. Federation*, **7**, 13-18 (in Japanese).
- Suzuki, Y. and I. Isozaki, 1994: On the development of a global ocean wave model JWA3G. *Proc. Pacific Ocean Remote Sensing Conf. in Melbourne, Australia*, 195-201.
- Sverdrup, H. U. and W. H. Munk, 1947: Wind sea and swell. Theory of relation for forecasting. *U.S. Navy Hydrogr. Office, Washington*, **No. 601**, 44pp.
- The SWAMP Group, 1985: *Ocean Wave Modeling*, Plenum Press, 256pp.
- Taira, K., 1975: Dynamics of ocean surface. *Lectures in Oceanography* 3, 2. Univ. of Tokyo Press, 47-83 (in Japanese).
- Takaishi, Y., T. Matsumoto and S. Ohmatsu, 1980: Winds and waves of the North Pacific Ocean. Supplement No. 3, *Papers Ship Res. Inst.*
- Toba, Y., 1972: Local balance in the air-sea boundary processes. I. On the growth process of wind waves. *J. Oceanogr. Soc. Japan*, **28**, 109-121.
- Toba, Y., 1973: Local balance in the air-sea boundary processes. III. On the spectrum of wind waves. *J. Oceanogr. Soc. Japan*, **29**, 209-220.
- Toba, Y., 1978: Stochastic form of the growth of wind waves in a single-parameter representation with physical implications. *J. Phys. Oceanogr.*, **8**, 494-507.
- Toba, Y., 1979: Study on wind waves as a strongly nonlinear phenomenon. *12th Symp. Naval Hydrodynamics, National Acad. Sci., Washington, D.C.*, 529-540.
- Toba, Y. and M. Chaen, 1973: Quantitative expression of the breaking of wind waves on the sea surface. *Rec. Oceanogr. Works in Japan*, **12**, 1-11.
- Toba, Y., S. Kawai and P. S. Joseph, 1985: The TOHOKU wave model. *Ocean Wave Modeling*, The SWAMP Group Ed., Plenum Press, 201-210.
- Toba, Y. and M. Koga, 1986: A parameter describing overall conditions of wave breaking, whitecapping, sea-spray production and wind stress. *Oceanic Whitecaps*, E. C. Monahan and G. Mac Niocaill, Eds., D. Reidel, 37-47.
- Toba, Y. and N. Ebuchi, 1991: Sea-surface roughness length fluctuating in concert with wind and waves. *J. Oceanogr. Soc. Japan*, **47**, 63-79.
- Tomita, H., I. Watanabe and K. Yazawa, 1992: On the statistics of ocean wave data on the North Pacific ocean. *Proc. 11th Ocean Eng. Symp., The Society Naval Arch. Japan*, 319-326.
- Townsend, W. F., J. T. McGoogan and E. J. Walsh, 1981: Satellite radar altimeters - Present and future oceanographic capabilities. *Oceanography from Space*, J. F. R. Gower, Ed., Plenum Press, N. Y., 625-636.
- Tsuruya, H., 1988: Experimental study on the wave decay in an opposing wind. *Coastal Eng. in Japan*, **30**, No. 2, 25-43.
- Uji, T., 1984: A coupled discrete wave model MRI- II. *J. Oceanogr. Soc. Japan*, **40**, 303-313.
- Ursell, F., 1956: Wave generation by wind. in *Survey in Mechanics*, Cambridge Univ. Press, 216-249.

- The WAMDI Group, 1988: The WAM model-A third generation ocean wave prediction model. *J. Phys. Oceanogr.*, **18**, 1775-1810.
- Webb, D.J., 1978: Non-linear transfers between sea waves. *Deep Sea Res.*, **25**, 279-298.
- Weber, S.L., 1994: Statistics of the air-sea fluxes of momentum and mechanical energy in a coupled wave-atmosphere model. *J. Phys. Oceanogr.*, **24**, 1388-1398.
- Wilson, B.W., 1961: Deep water wave generation by moving wind system. *Proc. ASCE*, **87**(WW2), 113-141.
- Wilson, B.W., 1965: Numerical prediction of ocean waves in the North Atlantic for December 1959. *Dtsch. Hydrogr. Zeit.*, **18**, 114-130.
- Wu, J., 1980: Wind stress coefficients over sea surface near neutral conditions: a Revisit. *J. Phys. Oceanogr.*, **10**, 727-740.
- Yamaguchi, M., Y. Tsuchiya, H. Oyada and K. Watanabe, 1979: Numerical ocean wave forecasting in the fetch limited area. *Proc. Coastal Eng., JSCE*, **26**, 96-100 (in Japanese).
- Yamanouchi, Y., 1989: Current topics on the ocean wave statistics. *Shipbuilding Technology and Development of the Ocean*, **4**, No.1 (in Japanese).
- Yamanouchi, Y. and A. Ogawa, 1970: Statistical diagrams on the winds and waves on the North Pacific Ocean. Supplement No.2, *Papers Ship Res. Inst.*
- Young, I.R., 1987: A general purpose spectral wave prediction model. *Research Report No.16, Univ. Coll. Australian Defence Force Acad.*, 24pp.
- Young, I.R., 1988: A shallow water spectral wave model. *J. Geophys. Res.*, **93**(C5), 5113-5129.
- Zambresky, L., 1989: A verification study of the global WAM model December 1987 - November 1988. *Technical Report No.63, ECMWF*, 86pp.

